ORIGINAL ARTICLE

Sensitivity analysis and estimation using a hierarchical Bayesian method for the parameters of the FvCB biochemical photosynthetic model

Tuo Han[1,2] · Gaofeng Zhu[1,2] · Jinzhu Ma[1,2] · Shangtao Wang[1,2] · Kun Zhang[1,2] · Xiaowen Liu[1,2] · Ting Ma[1,2] · Shasha Shang[1,2] · Chunlin Huang[3]

Abstract

Photosynthesis is a major process included in land surface models. Accurately estimating the parameters of the photosynthetic sub-models can greatly improve the ability of these models to accurately simulate the carbon cycle of terrestrial ecosystems. Here, we used a hierarchical Bayesian approach to fit the Farquhar–von Caemmerer–Berry model, which is based on the biochemistry of photosynthesis using 236 curves for the relationship between net CO_2 assimilation and changes in the intercellular CO_2 concentration. An advantage of the hierarchical Bayesian algorithm is that parameters can be estimated at multiple levels (plant, species, plant functional type, and population level) simultaneously. The parameters of the hierarchical strategy were based on the results of a sensitivity analysis. The Michaelis–Menten constant (K_{c25}), enthalpies of activation (E_J and E_V), and two optical parameters (θ and α) demonstrated considerable variation at different levels, which suggests that this variation cannot be ignored. The maximum electron transport rate (J_{max25}), maximum rate of Rubisco activity (V_{cmax25}), and dark respiration in the light (R_{d25}) were higher for broad-leaved plants than for needle-leaved plants. Comparison of the model's simulated outputs with observed data showed strong and significant positive correlations, particularly when the model was parameterized at the plant level. In summary, our study is the first effort to combine sensitivity analysis and hierarchical Bayesian parameter estimation. The resulting realistic parameter distributions for the four levels provide a reference for current and future land surface models. Furthermore, the observed variation in the parameters will require attention when using photosynthetic parameters in future models.

Keywords Photosynthesis · FvCB model · Sensitivity analysis · Hierarchical Bayesian analysis · Plant level · Species level · Plant functional type level · LSMs

✉ Gaofeng Zhu
zhugf@lzu.edu.cn

1   Key Laboratory of Western China's Environmental Systems (Ministry of Education), Lanzhou University, Tianshui Road 222, Lanzhou 730000, Gansu, People's Republic of China

2   College of Earth and Environmental Sciences, Lanzhou University, Lanzhou, China

3   Key Laboratory of Remote Sensing of Gansu Province, Cold and Arid Regions Environmental and Engineering Research Institute, Chinese Academy of Sciences, Lanzhou 730000, China

Introduction

Photosynthesis is the process by which plants take up carbon. It is therefore both an integral part of the terrestrial ecosystem carbon cycle (Luo et al. 2003; Trudinger et al. 2007; Fox et al. 2009) and a decisive factor in the development of plant biomass (Amane 2011; Fischer et al. 2014). Thus, studies of photosynthetic processes have drawn much attention in many fields, including climate change and agronomy (Sellers et al. 1997; Pitman 2003; Medlyn et al. 2011; Fisher et al. 2014). For more than a century, various models of photosynthesis have been developed, ranging from equations driven by several limited factors (Blackman 1905) to empirical models such as the Michaelis–Menten model (Michaelis and Menten 1913), the rectangular hyperbolic model (Baly 1935), the

non-rectangular hyperbolic model (Thornley 1976), and mechanistic models (i.e., Farquhar et al. 1980; Collatz et al. 1991). Among them, the model proposed by (Farquhar et al. 1980) (hereafter, the FvCB model) was based on a rigorous consideration of biochemical mechanisms, and as a result has been widely used in many land surface models, such as SiB2 (Sellers et al. 1995a, b), CLM (Bonan et al. 2011), BIOME-BGC (Running and Hunt 1993), and ECOSYS (Hansen et al. 2005).

However, to improve the simulation accuracy of photosynthesis, the parameters in the FvCB model must be properly identified and estimated. Bonan et al. (2011) pointed out that the uncertainty in the Community Land Model (CLM4) estimates of the gross primary production (GPP) due to uncertainty in the photosynthetic parameters would be about equal to the uncertainty that derives from structural errors in the model. Due to the high nonlinearity and noncontinuity of the FvCB model, many researchers have looked for effective optimization methods (Dubois et al. 2007; Sharkey et al. 2007; Xu et al. 2012). Unfortunately, researchers have not reached an agreement on how many parameters in the model and which ones must be estimated more accurately. For example, Zhu et al. (2011) estimated all the parameters in the FvCB model, whereas other researchers selected only a few parameters: the maximum rate of Rubisco activity (V_{cmax}), the maximum electron transport rate (J_{max}), triose phosphate limitation (TPU), dark respiration (R_d), and mesophyll conductance (g_m) (Miao et al. 2009) or just V_{cmax}, J_{max}, g_m, and R_d (Su et al. 2009). Thus, it's necessary to improve our understanding of the behavior of the parameters in the FvCB model and identify the parameters that are most sensitive to environmental factors and vegetation characteristics.

Sensitivity analysis is a powerful method to identify the key parameters that determine the performance of a model (Tang et al. 2007a; Wang et al. 2013) and has been widely used in many fields, including economics and the physical, social, and environmental sciences. Of the various sensitivity analysis methods that have been developed, the Morris method (Morris 1991) and the Sobol' method (Sobol' 1993) have proven to be effective and are broadly used. The Morris method is an one-factor-at-a-time method that provides a qualitative analysis with low computational requirements. The Sobol' method is a variance-based method that can globally characterize single parameter and multiparameter interactive sensitivities (Fu et al. 2011). In previous studies, these methods have been applied mainly to complex hydrological, and environmental models (Nossent et al. 2011; Han and Zheng 2016). Although, there are several prior studies that have involved sensitivity analyses of photosynthesis scheme (Zaehle et al. 2005; Walker et al. 2018), it is not yet known if the sensitive parameters that have significant influence on the model performance are the same in different plant functional types. Thus, the sensitivity analysis in

the FvCB model should be applied across a wider range of species and environmental conditions.

Subsequently, due to the significant role that the key parameters play in the FvCB model and land surface models, it is essential to estimate their values accurately. However, previous studies showed that estimates of the model's photosynthetic parameters were influenced by the estimation method, which included least-squares regression (Harley et al. 1992; Dubois et al. 2007; Miao et al. 2009; Qian et al. 2012), genetic algorithms (Su et al. 2009), and the Bayesian method (Zhu et al. 2011). More importantly, these parameters were confirmed to vary among plants, species, plant functional types, and bimoes (Pitman 2003; Patrick et al. 2009; Galmés et al. 2014; Hermida-Carrera et al. 2016). To simultaneously obtain proper ranges of values for the model parameters in different levels, the hierarchical Bayesian approach is suitable because its hierarchical approach can account for the hierarchy of these levels, such as individual plants being nested within a species, and a species being nested within a functional type (Clark 2005). Specially, the hierarchical structure permits analysis of multiple data types within a single analysis. Data sets from diverse sources (i.e., a set of CO_2 response curve data) can exchange information, which makes full use of available data. It can also mitigate the effects of measurement errors in the observed data. Recently, more and more studied proved that the HB method provides powerful tools for optimizing model parameters and quantifying uncertainties (Norros et al. 2017; Su et al. 2018). Patrick et al. (2009) and Feng and Dietze (2013) have ever used the HB method to optimize model parameters of the FvCB model, and confirmed the HB method had great potential to improve the estimation of photosynthetic parameters in different levels. Nevertheless, photosynthetic data used in Patrick et al. (2009) just involved shrub species in a specific desert ecosystem in North America, while Feng and Dietze (2013) mainly focused on the variations of some key parameters (i.e., V_{cmax}/V_{max}, J_{max}/k, a, and R_d) of 25 grassland species. Among all parameters in the FvCB model, which parameters and how these parameters varied in different environmental conditions and plant functional types have not yet been known, and need to be pay more attentions.

In this study, our goal is to identify the key parameters in the FvCB model and estimate their values at different hierarchical levels across a wide range of species. To do so, we obtained 236 curves for the relationship between net CO_2 assimilation and changes in the intercellular CO_2 concentration (i.e., the A/C_i curves) for 51 C_3 species. The specific objectives were (1) to identify the sensitive parameters using the Morris and the Sobol' methods, (2) to estimate the values of the key photosynthetic parameters at the level of plants, species, and plant functional types using the hierarchical Bayesian method, and (3) to assess the variation of these parameters at these three levels. In this context, we address

the following questions: among all the parameters in the FvCB model, which parameters have significant influence on the model performance? then, if the parameters (e.g., Michaelis–Menten constant: K_{c25}, K_{o25}; enthalpies of activation E_J, E_V, E_R, and E_g; or optical parameters θ, and α) commonly used as constant values are variable within and/or across a broad plant functional types, species, and plants; and what are the distributions of these parameter values in different levels? Moreover, if there are significant differences in simulation accuracy when using parameter values of different levels (e.g., plant functional types, species level, and plant level)?

Materials and methods

This section consists of four major components. First, we describe our formulation of the FvCB model, including information on how the model is driven, its structure, and its parameters). Next, we introduce the two sensitivity analysis methods and explain how they reveal the most sensitive parameters. Third, we clarify the hierarchical structure based on the model's structure and the results of the sensitivity analysis. Last, we describe our data sources and performance metrics.

The FvCB model

The FvCB model was developed by Farquhar et al. (1980) and refined by other scholars (von Caemmerer and Farquhar 1981; Bernacchi et al. 2001; Long and Bernacchi 2003). It can be described as follows:

$$A_n = \min\{A_c, A_j\} \tag{1}$$

where A_n is the net photosynthetic rate (µmol m^{-2} s^{-1}), and A_c and A_j are the net photosynthetic rates limited by Rubisco and RuBP, respectively (µmol m^{-2} s^{-1}). We did not account

for triose phosphate limitation (TPU) because this phase rarely limits photosynthesis and TPU limitation was uncommon in field observations (Medlyn and Dreyer 2002; Patrick et al. 2009; Feng and Dietze 2013).

$$A_c = V_{c\,max}\left[\frac{C_c - \Gamma^*}{C_c + K_c(1 + o/K_o)}\right] - R_d \tag{2}$$

$$A_j = \frac{J(C_i - \Gamma^*)}{4C_i + 8\Gamma^*} - R_d \tag{3}$$

$$C_c = C_i - \frac{A}{g_m} \tag{4}$$

$$\theta J^2 - (I + J_{max})J + IJ_{max} = 0 \tag{5}$$

$$I = I_0 \times \alpha \times (1 - f)/2 \tag{6}$$

where V_{cmax} is the maximum rate of Rubisco activity (µmol m^{-2} s^{-1}); C_c and o mean the partial pressure of carbon dioxide and oxygen, respectively (Pa); Γ^* means the CO_2 compensation point when mitochondrial respiration is zero (Pa); K_c and K_o are the Michaelis–Menten constants for carboxylation and oxygenation, respectively (kPa or Pa); J is the electron transport rate in the RuBP-limited stage (µmol m^{-2} s^{-1}); C_i is the intercellular CO_2 concentration (µmol mol^{-1}); R_d means the leaf dark respiration in the light (µmol m^{-2} s^{-1}); and A means photosynthetic rate (µmol m^{-2} s^{-1}). θ means the curvature (convexity) of the light-response curve; I means the photosynthetically active light absorbed by PSII (µmol m^{-2} s^{-1}); J_{max} means the maximum electron transport rate (µmol m^{-2} s^{-1}); g_m represents the mesophyll conductance (µmol m^{-2} s^{-1} Pa^{-1}; Harley and Sharkey 1991; Sharkey et al. 2007); I_0 is the total incident irradiance (µmol m^{-2} s^{-1}); α means the leaf absorbance (von Caemmerer 2000); and f is a correction factor for spectral quality (equal to about 0.15; Evans 1987).

The three enzyme kinetics parameters (K_c, K_o, and Γ^*) can be described as follows (Bernacchi et al. 2001, 2002):

$$\text{parameter}\ (K_c, K_o, \Gamma^*) = K_{25}\exp\left[E_a\left(T_k - 298\right)\right]/\left(298RT_k\right) \tag{7}$$

where K_{25} is the value of K_c, K_o, or Γ^* at 25 °C (Pa or kPa); E_a (i.e., E_{Kc}, E_{Ko}, E_{Γ^*}) is the activation energy (enthalpy; J mol^{-1} or kJ mol^{-1}) for the three K parameters; and T_k means the leaf temperature (in K). The four temperature dependence parameters (J_{max}, V_{cmax}, R_d, and g_m) can be expressed using the Arrhenius function (Harley et al. 1986, 1992; Lloyd et al. 1992; Medlyn and Dreyer 2002):

$$\text{parameter}\left(J_{max}, V_{cmax}, R_d, \text{and}\, g_m\right) = K_{25}\exp\left\{E_a\left(T_k - 298\right) / \left(298RT_k\right)\right\} \tag{8}$$

where K_{25} is the value of V_{cmax}, J_{max}, R_d, or g_m at 25 °C and E_a (i.e., the enthalpies of activation; E_J, E_V, E_R, E_g) is the rate of exponential increase of the function. The FvCB model uses a total of 16 parameters, which are summarized in Table 1.

Sensitivity analysis methods

The Morris method

The Morris (1991) method is a global sensitivity analysis method that provides a qualitative ranking of the sensitivity

Table 1 Parameters and prior ranges of the FvCB model

Process parameter	Range	Units	Description	References
J_{max25}	(30.3, 200)	µmol m^{-2} s^{-1}	Potential light-saturated electron transport rate at 25 °C	Medlyn and Dreyer (2002), Kattge and Knorr (2007), Patrick et al. (2009)
V_{cmax25}	(24.3, 200)	µmol m^{-2} s^{-1}	Maximum carboxylation rate allowed by Rubisco at 25 °C	Medlyn and Dreyer (2002), Kattge and Knorr (2007), Patrick et al. (2009)
R_{d25}	(0.01, 10)	µmol m^{-2} s^{-1}	Leaf dark respiration in the light at 25 °C	Sharkey et al. (2007), Su et al. (2009), Zhu et al. (2011)
g_{m25}	(0.03, 10)	µmol m^{-2} s^{-1} P$_a^{-1}$	Mesophyll conductance at 25 °C	Ethier and Livingston (2004), Sharkey et al. (2007), Su et al. (2009)
K_{c25}	(24.8, 58.4)	P$_a$	K_c at 25 °C	Sharkey et al. (2007), von Caemmerer et al. (1994), Patrick et al. (2009)
K_{o25}	(15.8, 50.4)	kP$_a$	K_o at 25 °C	Sharkey et al. (2007), von Caemmerer et al. (1994), Patrick et al. (2009)
Γ^*_{25}	(2, 10)	P$_a$	Γ^* at 25 °C	Sharkey et al. (2007), von Caemmerer (2000)
E_J	(35.9, 120.6)	kJ mol^{-1}	Activation energy of J_{max}	Kattge and Knorr (2007), Leuning (1997, 2002), Medlyn and Dreyer (2002), Sharkey et al. (2007)
E_V	(51.3, 128.4)	kJ mol^{-1}	Activation energy of V_{cmax}	Kattge and Knorr (2007), Leuning (1997, 2002), Medlyn and Dreyer (2002), Sharkey et al. (2007)
E_R	(41.1, 92.6)	kJ mol^{-1}	Activation energy of R_d	Patrick et al. (2009)
E_g	(20, 100)	kJ mol^{-1}	Activation energy of g_m	Sharkey et al. (2007), Patrick et al. (2009)
E_{Kc}	(54.6, 104)	kJ mol^{-1}	Activation energy of K_c	Ethier and Livingston (2004), Sharkey et al. (2007), von Caemmerer (2000)
E_{Ko}	(9.3, 36.3)	kJ mol^{-1}	Activation energy of K_o	Ethier and Livingston (2004), Sharkey et al. (2007), von Caemmerer (2000)
E_{Γ^*}	(23.5, 37.2)	kJ mol^{-1}	Activation energy of Γ^*	Bernacchi et al. (2001), Ethier and Livingston (2004), Sharkey et al. (2007)
θ	(0.15, 1)	–	Light-response curvature	Patrick et al. (2009)
α	(0.15, 1)	mol mol^{-1}	Leaf absorbance	Patrick et al. (2009)

of the parameters. In this method, the parameter range is normalized as a uniform distribution within [0, 1] and discretized into a **p**-level grid $\boldsymbol{\Omega} = \{0, 1/(\boldsymbol{p}–1), 2/(\boldsymbol{p}–1), 3/(\boldsymbol{p}–1), …, 1\}$. At a randomly selected point in $\boldsymbol{\Omega}$, the elementary effect (*EE*) of the *i*th parameter is:

$$\mathrm{EE}_i(\vec{\theta}, \Delta) = \frac{f(\theta_1^*, …, \theta_i^* + \Delta, …, \theta_n^*) - f(\theta_1^*, …, \theta_i^*, …, \theta_n^*)}{\Delta}$$

(9)

where $\vec{\theta}$ is the *n*-dimensional vector of parameter sets, $(\boldsymbol{\theta}_1^*, \boldsymbol{\theta}_2^*, …, \boldsymbol{\theta}_n^*)$ is a randomly selected point in $\boldsymbol{\Omega}$, and Δ is the fixed increment ($\boldsymbol{p}/[2(\boldsymbol{p}–1)]$), the function *f* means goodness-of-fit metrics or relevant model outputs, and $\mathrm{EE}_i(\vec{\theta},\Delta)$ means the change in output *f* caused by a change in the *i*th parameter. To compute the values of EE for each parameter, $n+1$ simulations (i.e., a simulation for the selected point plus *n* simulations for the fixed increment Δ for the *n* parameters) are conducted to complete a "trajectory". If the number of trajectories is *q*, we have *q* values of EE for each parameter with $q(q+1)$ simulations. Using the ensemble of EE values, it's possible to describe the statistical characteristics of a

parameter's sensitivity: the mean of EE (μ), the standard deviation of EE (σ), and the mean absolute EE (|EE|)]. The mean EE reflects a parameter's overall effect, whereas the standard deviation of EE indicates the strength of the parameter's nonlinearity or its interactions with other parameters. The mean absolute EE reveals the non-influential factor (i.e., a low mean absolute EE represents a less-important parameter), which can be used to rank parameter sensitivity (Campolongo et al. 2007; Han and Zheng 2016). In the present study, the grid level (*p*) was set to 6 and chose a trajectory number (*q*) of 500 (Gálvez and Capuz-Rizo 2016). Additionally, all the parameters in $\vec{\theta}$ were assumed to follow uniform distributions, whose feasible ranges were listed in Table 1. The proposed ranges were mainly based on the default ranges in references.

The Sobol′ method

In contrast with the Morris method, the Sobol′ method is a quantitative sensitivity analysis method based on variance decomposition (Sobol′ 1990, 2001). The variance of certain

goodness-of-fit metrics or relevant model outputs can be decomposed into variances derived from both individual parameters and their interactions. The total variance $D(f)$ can be decomposed into a series of summations of increasing dimensionality:

$$D(f) = \sum_i D_i + \sum_{i<j} D_{ij} + \sum_{i<j<k} D_{ijk} + \cdots + D_{12\ldots n} \tag{10}$$

where f means a specific goodness-of-fit metric or relevant model output chosen by the researcher; D_i is the amount of deviation of the ith parameter $\boldsymbol{\theta}_i$; D_{ij} is the partial variance result from the interaction of $\boldsymbol{\theta}_i$ and $\boldsymbol{\theta}_j$; and n is the total number of parameters. In this method, the sensitivity of a single parameter or of parameter interactions can be evaluated by their percentage contribution to the total variance (D) in the form of two sensitivity indexes:

$$\text{First}-\text{order index}: S_i = D_i/D \tag{11}$$

$$\text{Total}-\text{order index}: S_{\text{T}i} = 1 - \left(D_{\sim i}/D\right) \tag{12}$$

where S_i indicates the contribution derived from the main effect of $\boldsymbol{\theta}_i$, $S_{\text{T}i}$ means both the influence of $\boldsymbol{\theta}_i$ and the influence of its interactions with all the other parameters, and $D_{\sim i}$ means the amount of deviation of all parameters other than $\boldsymbol{\theta}_i$. By analyzing the difference between $S_{\text{T}i}$ and S_i, we can assess the impact of the interaction between parameter $\boldsymbol{\theta}_i$ and the other parameters.

The high dimensionality and nonlinearity of the FvCB model made it difficult to directly obtain analytical integrals of variances. To solve that problem, we calculated the variances in Eq. (10) using Monte Carlo integrations which was found to be effective (Sobol' 1993). The Monte Carlo approximations for D, D_i, and $D_{\sim i}$ are given in the following equations as presented in previous studies (Sobol' 1993; Hall et al. 2005):

$$f_0 = \frac{1}{s} \sum_{k=1}^{s} f(\boldsymbol{\theta}_k) \tag{13}$$

$$D = \frac{1}{s} \sum_{k=1}^{s} f^2(\boldsymbol{\theta}_k) - f_0^2 \tag{14}$$

$$D_i = \frac{1}{s} \sum_{k=1}^{s} f(\boldsymbol{\theta}_k^{(a)}) f(\boldsymbol{\theta}_{(\sim i)k}^{(b)}, \boldsymbol{\theta}_{ik}^{(a)}) - f_0^2 \tag{15}$$

$$D_{\sim i} = \frac{1}{s} \sum_{k=1}^{s} f(\boldsymbol{\theta}_k^{(a)}) f(\boldsymbol{\theta}_{(\sim i)k}^{(a)}, \boldsymbol{\theta}_{ik}^{(b)}) - f_0^2 \tag{16}$$

where the variable s represents the Monte Carlo sample size, $\boldsymbol{\theta}_k$ represents the sampled individual in the scaled unit hypercube, and superscripts (a) and (b) are two different samples. Parameters with values drawn from sample (a) can be denoted by $\boldsymbol{\theta}_k^{(a)}$. The symbols $\boldsymbol{\theta}_{ik}^{(a)}$ and $\boldsymbol{\theta}_{ik}^{(b)}$ donated cases when parameter $\boldsymbol{\theta}_k$ draws values from sample (a) and (b), respectively, and $\boldsymbol{\theta}_{(\sim i)k}^{(a)}$ and $\boldsymbol{\theta}_{(\sim i)k}^{(b)}$ represented cases when all of the parameters except for $\boldsymbol{\theta}_k$ use the sampled values in sample (a) and (b), respectively. In this study, we chose the Latin hypercube sampling (LHS) method to obtain samples (McKay et al. 2000; Sieber and Uhlenbrook 2005). The method segments the parameter space into N ranges, and each range was sampled only once. This ensures that every portion of the parameter space was taken into account (Helton and Davis 2003; Kucherenko et al. 2009). Then, N samples are generated for each parameter. Here, N was set to 10,000. The process can be repeated n (number of parameters, equal to 16) times for all parameters, such that a total of $N \times n$ ($= 10,000 \times 16$) random sample combinations were generated. More detailed description of the implemented computational process of LHS can refer the following papers (Hall et al. 2005; Zhang et al. 2013). Moreover, feasible ranges for each parameter used in this method were the same as the ranges in the Morris method (Table 1). Based on the sensitivity index, we defined thresholds to differentiate among parameters with different sensitivity: highly sensitive parameters had to account for an average of at least 10% of the overall model variance (i.e., a threshold of 0.10), vs. 1% for sensitive parameters (i.e., a threshold of 0.01). When the contributions to the overall model variance were less than 0.01, we considered the parameters to be insensitive (Tang et al. 2007a, b). This threshold has been widely used in previous research based on the Sobol' method (Cibin et al. 2010; Gálvez and Capuz-Rizo 2016; Zhang et al. 2017).

Goodness-of-fit metrics

In both the Morris method and the Sobol' method, the direct model output (f) is replaced by a model goodness-of-fit metric (Nossent et al. 2011). Here, we chose the root-mean-square error (RMSE):

$$\text{RMSE} = \sqrt{\frac{1}{m} \sum_{r=1}^{m} (A_{\text{nobs}}(r) - A_{\text{nsim}}(r))^2} \tag{17}$$

where m is the total number of input data, and $A_{\text{nobs}}(r)$ and $A_{\text{nsim}}(r)$ are observed and simulated net photosynthetic rate of the rth data. To confirm the practicality and reliability of our sensitivity analysis results for both the Morris method and the Sobol' method using the RMSE metric for the FvCB model, we tested two additional goodness-of-fit metrics: the Nash–Sutcliffe efficiency (NSE) and the *Bias* (Details of these metrics are provided in the Supplementary Material). The procedures of the Morris and Sobol' method

were written in the computer programming language Matlab 2015a (Detail code was provided in the text 'Model Code').

Hierarchical Bayesian model of photosynthesis

We used the hierarchical Bayesian framework to estimate the values of the key parameters by fitting the FvCB model to photosynthetic data in the form of A/C_i curves (Clark 2007). This method can (1) estimate all parameters simultaneously, after considering both observation error and parameter uncertainty (Carlin et al. 2006); (2) incorporate multiple gas-exchange datasets simultaneously instead of fitting them curve by curve, and can therefore strengthen the results and improve model performance, especially with limited data; (3) estimate parameters in the form of posterior probability distributions rather than as single values; and (4) partition uncertainty into multiple processes, thereby improving our understanding of the model mechanisms.

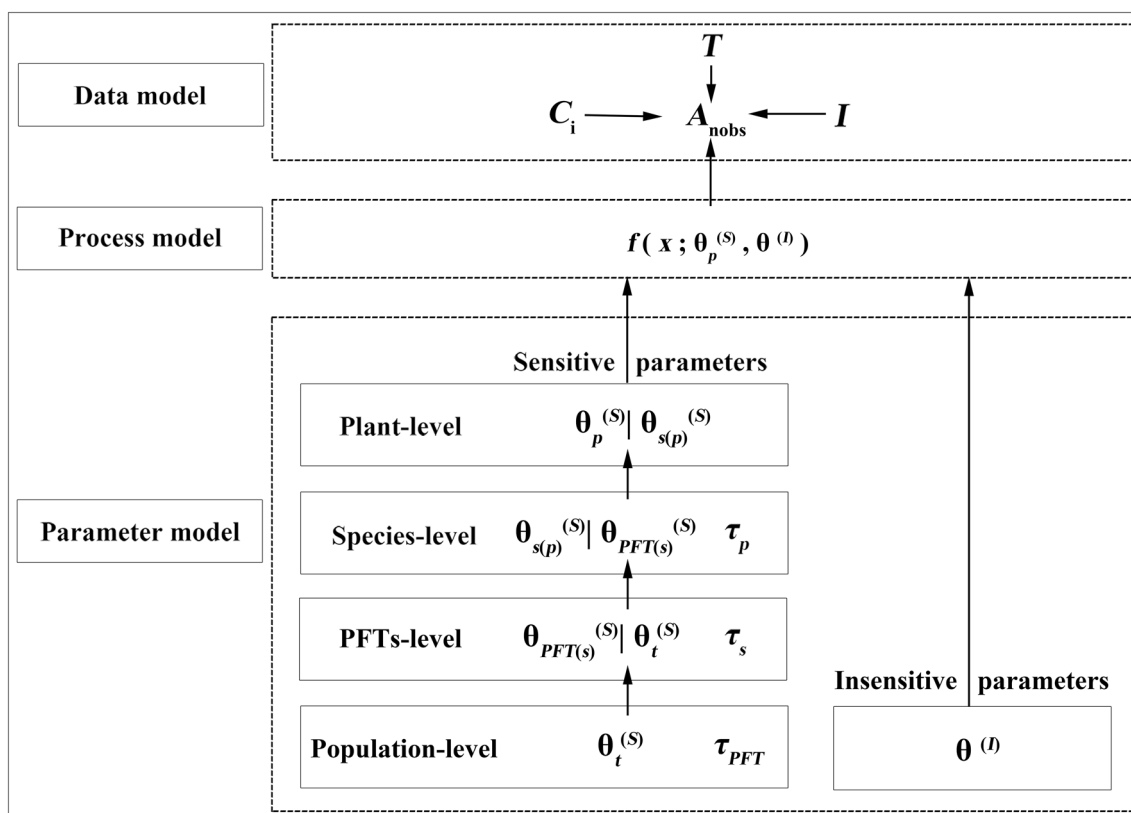This method accommodates complexity by dissecting the analytical procedure into three primary components: the data

model, the process model, and the parameter model (Fig. 1). The data model describes the likelihood function for the observed net photosynthetic rate, which was assumed to be normally distributed around the simulated net photosynthetic rate, and can be expressed as:

$$A_{nobs} \sim \textbf{Normal}(A_{nsim}, \tau) \qquad (18)$$

where A_{nobs} is the observed net photosynthetic rate (μmol m^{-2} s^{-1}); A_{nsim} is the simulated net photosynthetic rate based on the FvCB model (μmol m^{-2} s^{-1}); and τ is the precision ($= 1/$variance) parameter, which reflects the variation of measurement errors.

The process model specifies the biochemical processes according to the FvCB model and predicted the simulated net photosynthesis based on observed data [T (represents the temperature in °C), I, and C_i] and all model parameters.

The parameter model specifies the prior distributions for the parameters used in the process model. According to the results of our sensitivity analysis, we classified the 16 parameters into two types: sensitive parameters (i.e., $\theta^{(S)}$) and insensitive parameters (i.e., $\theta^{(I)}$). For the sensitive

Fig. 1 Hierarchical Bayesian parameterization of the FvCB model. In the data model, A_{nobs} (observed net photosynthetic rates), C_i (internal CO$_2$ concentration), T (temperature in °C), and I (the photosynthetically active light absorbed by PSII) are input datasets. The process model describes parameters and model structure related to biochemi-

cal process of photosynthesis. The parameter model includes hierarchical priors for each parameter. $\theta^{(S)}$ and $\theta^{(I)}$ are the sensitive and insensitive parameters, respectively. τ_p, τ_s and τ_{PFT} are the precision (1/variance) parameter which represents variation in plant, species, and PFTs, level, respectively

parameters, we designed a nested and hierarchical structure (Fig. 1), in which we allowed the sensitive parameters to vary at four hierarchical levels (i.e., plant, species, and plant functional type, and population level) and to exchange information within and across levels (Carlin et al. 2006). Based on this framework, we assumed that the plant-level parameters, which were directly relevant to the individual A/C_i curves, were nested within species, and that the species-level parameters were nested within the plant functional types. That is, sensitive plant-level parameters ($\theta_p^{(S)}$) were assumed to be nested within species, such that:

$$\theta_p^{(S)} \sim \text{Normal}(\theta_{s(p)}^{(S)}, \tau_p) \tag{19}$$

where $\theta_{s(p)}^{(S)}$ represents the means of the species-level parameters for species s and τ_p represents the precision ($= 1/\text{variance}$) parameter that describes variability between individual plants or the curves within a species. Additional species-level parameters varied around the plant function type parameters, such that:

$$\theta_{s(p)}^{(S)} \sim \text{Normal}(\theta_{\text{PFT}(s)}^{(S)}, \tau_s) \tag{20}$$

where $\theta_{\text{PFT}(s)}^{(S)}$ and τ_s represent the mean at the plant function type level and the corresponding precision parameter for variation among species, respectively. Note that τ_s describes species-to-species variability within a plant function type. The plant function type level parameters varied around the population-level parameters, such that:

$$\theta_{\text{PFT}(s)}^{(S)} \sim \text{Normal}(\theta_t^{(S)}, \tau_{\text{PFT}}) \tag{21}$$

where $\theta_t^{(S)}$ and τ_{PFT} are the population-level mean and precision parameters for variation among plant functional types, respectively. Note that τ_{PFT} describes variability among plant functional types within the C_3 metabolic category for all sites included in our study.

For the insensitive parameters ($\theta^{(I)}$), we assigned non-hierarchical priors (Fig. 1). Although the two Rubisco kinetics parameters at 25 °C (K_{o25} and Γ_{25}^*) and the activation energy parameters (E_R, E_g, E_{Kc}, E_{Ko}, and $E_{\Gamma*}$) are usually assumed to be constants across a wide range of C_3 species (von Caemmerer 2000), we hypothesized that they instead vary at the level of plant functional types. We employed slightly informative normal prior distributions with mean values (θ_0) and small precision (τ_0):

$$\theta_{\text{PFT}}^{(I)} \sim \text{Normal}(\theta_0, \tau_0) \tag{22}$$

Finally, we must specify the distributions for the hyper-prior parameters (i.e., $\theta_t^{(S)}$, τ_{PFT}, τ_s, τ_p and τ) to complete the model hierarchy. Standard, relatively diffuse distributions are employed for the hyper-prior parameters, which ensure

the feasible parameter ranges were big enough to determine their values (Gelman 2006). Here, we specified a normal density with a large variance for these population-level mean parameters ($\theta_t^{(S)}$). For the variance parameters, we chose folded Cauchy densities to generate the priors (Gelman 2004, 2006). Detail information of each prior distribution were listed in the Supplementary Material.

By combining the three parts of the model, we generated posterior probability density functions for all parameters. The hierarchical Bayesian model was implemented in version 3.2.3 of the OpenBUGS statistical software (http://www.openbugs.net/w/FrontPage). In this method, many chains could run in parallel, thereby greatly improving the search efficiency for parameter posterior distributions. We ran three Markov-chain Monte Carlo chains for 50,000 steps each, discarding the first 5000 steps for burn-in in every chain. The remaining samples were tested for convergence of each chain using the BGR diagnostic tool (Gelman 2004). Details of the hierarchical Bayesian model and the parameterization process are provided in the text 'Model Code'.

Datasets

The photosynthetic data used in this paper came from 23 field sites (Table 2), and had been collected by the Wright Lab (De Kauwe et al. 2016). These sites provided 236 A/C_i curves from 51 C3 species on four continents (Asia, Europe, North America, and Oceania) and represent six typical plant functional types that follow the Simple Biosphere model version 2 (SiB2) classification: agriculture/C_3 grassland (AGG), broadleaf-deciduous trees (BDT), broadleaf-evergreen trees (BET), dwarf trees and shrubs (DTS), needleleaf-deciduous trees (NDT), and needleleaf-evergreen trees (NET). In most cases, gas-exchange measurements were conducted using the Li-6400 portable photosynthetic system (Li-Cor, Lincoln, NE, USA) (Ellsworth et al. 2015).

Performance metrics

The performance of the FvCB model whose parameters we parameterized was quantified by using the RMSE metric, calculated using Eq. (13) and Pearson's correlation coefficient (R) which was computed as follows:

$$R = \frac{\sum_{r=1}^{m} (A_{\text{nobs}}(r) - \overline{A_{\text{nobs}}})(A_{\text{nsim}}(r) - \overline{A_{\text{nsim}}})}{\sqrt{\sum_{r=1}^{m} \left(A_{\text{nobs}}(r) - \overline{A_{\text{nobs}}}\right)^2 \cdot \sum_{r=1}^{m} \left(A_{\text{nsim}}(r) - \overline{A_{\text{nsim}}}\right)^2}} \tag{23}$$

Table 2 Details of the data used in this study. Note that negative latitudes are in the southern hemisphere, and negative longitudes are in the western hemisphere

Site number	Site name	Latitude (°N)	Longitude (°E)	Biome type	PFT	Species
1	Kuringgai Murrua-track	−33.69	151.14	Temperate heath	DTS	*Hakea dactyloides*; *Banksia mariana*; *Hakea teretifolia*; *Banksia oblongifolia*
		−32.70	151.14	Temperate heath	DTS	*Banksia oblongifolia*
		−33.69	151.14	Temperate heath	BET	*Eucalyptus haemastoma*
2	Duke Forest (FACE)	35.98	−79.09	Temperate evergreen forest	NET	*Pinus taeda*
3	Duke Forest, NC, USA	35.98	−79.09	Temperate evergreen forest	NET	*Pinus virginiana*
		35.97	−79.10	Temperate deciduous forest	BDT	*Liquidambar styraciflua*; *Liriodendron tulipifera*; *Quercus alba*; *Carya tomentosa*
4	Cedar Creek LTER	45.41	−93.19	Temperate deciduous forest	BDT	*Quercus macrocarpa*
5	Cedar Creek LTER/BIOCON FACE	45.40	−93.18	Temperate grassland or prairie	AGG	*Lupinus perennis*; *Lespedeza capitata*
					AGG	*Solidago rigida*; *Anemone cylindrica*; *Achillea millefolium*
					AGG	*Agropyron repens*; *Bromus inermis*; *Poa pratensis*
6	Nevada Test site FACE	36.77	−115.97	Desert	AGG	*Oenothera perennis*
					DTS	*Larrea tridentata*
7	Nevada Test Site, NV, USA	36.77	−115.97	Desert	DTS	*Ambrosia dumosa*
					DTS	*Krameria parvifolia*
8	Aspen FACE	45.68	−89.63	Temperate deciduous forest	BDT	*Populus tremuloides*; *Acer saccharum*; *Betula papyrifera*
9	Carolina Lake	35.90	−79.09	Temperate deciduous forest	NDT	*Taxodium distichum*
10	Carolina Beach, NC, USA	34.05	−77.91	Temperate coastal forest	BET	*Quercus virginiana*
11	Saginaw forest, MI, USA	42.27	−83.81	Temperate deciduous forest	AGG	*Podophyllum peltatum*
12	UMBS Pellston, MI, USA	45.56	−84.72	Temperate deciduous forest	BDT	*Acer rubrum*; *Populus grandidentata*
13	Endla bog, Endla, Estonia	58.86	26.17	Boreal coniferous forest	NET	*Pinus sylvestris*
14	Hawkesbury, Richmond, NSW, Australia	−33.61	150.01	Temperate tree plantation	BET	*Eucalyptus globulus*; *Eucalyptus saligna*; *Eucalyptus dunnii*; *Eucalyptus melliodora*;
15	Blue Mountains, NSW, Australia	−33.71	150.55	Sclerophyll woodland	DTS	*Persoonia levis*
					BET	*Syncarpia glomulifera*; *Acacia obtusifolia*; *Banksia serrata*
16	Cape Tribulation crane site, Queensland, Australia	−16.10	145.45	Tropical rainforest	BET	*Syzygium sayeri*
17	La Sueur National Park, WA, Australia	−30.19	115.14	Mediterranean (Kwongan) woodland	BET	*Eucalyptus todtiana*; *Banksia attenuata*
18	Driftway Cumberland Plain, Richmond, NSW	−33.62	150.74	Sclerophyll woodland	BET	*Eucalyptus tereticornis*
19	Cocoparra National Park	−34.17	146.23	Sclerophyll woodland	DTS	*Hakea tephrosperma*
					BET	*Eucalyptus populnea*
20	Illawarra, Robertson, NSW, Australia	−34.62	150.71	Warm-temperate forest	BET	*Eucalyptus fastigata*
21	EucFACE site	−33.62	150.74	Temperate grassy woodland	AGG	*Microlaena* sp.
22	Mill Haft forest, UK	52.81	−2.30	Deciduous forest	BDT	*Quercus robur*
23	Edgbaston wood, UK	52.81	−2.30	Deciduous forest	BDT	*Fagus sylvatica*

Plant functional types (PFTs) based on the Simple Biosphere model version 2 (SiB2) classification: *AGG* agriculture/C3 grassland, *BDT* broadleaf-deciduous trees, *BET* broadleaf-evergreen trees, *DTS* dwarf trees and shrubs, *NDT* needleleaf-deciduous trees, *NET* needleleaf-evergreen trees

where $\overline{A_{\text{nobs}}}$ and $\overline{A_{\text{nsim}}}$ are the mean of the observed and simulated net photosynthetic rates, respectively. We also used the Nash–Sutcliffe efficiency (*NSE*) and the *Bias* goodness-of-fit metrics to validate the results using *RMSE*. Details of these two additional metrics are provided in the Supplementary Material. Additionally, model comparison was quantified using Deviance Information Criterion (DIC), details about the method can be found in the Supplementary Material, and also available in Spiegelhalter et al. (2002).

Results

Parameter sensitivity analysis

Figure S1 and Table S1 present the results of the sensitivity analysis using the Morris method. Not surprising, two parameters (the maximum electron transport rate at 25 °C, J_{max25}, and the maximum rate of Rubisco activity at 25 °C, V_{cmax25}) were the most sensitive across all plant functional types. The dark respiration in the light (R_{d25}), mesophyll conductance (g_{m25}), and Michaelis–Menten constant (K_{c25}) at 25 °C, as well as the enthalpy of activation for J_{max} (E_{J}) and V_{cmax} (E_{V}), the light-response curvature (θ), and absorbance (α), which were distributed in the intermediate region of the graphs in Fig. S1, were sensitive parameters. The other parameters, with sensitivities distributed around zero, were insensitive. Table 3 shows the ranks of the 10 most sensitive parameters based on the mean |EE|. Obviously, J_{max25}, V_{cmax25}, R_{d25}, and g_{m25} were the four most sensitive parameters across all plant functional types. The mean |EE| values for J_{max25} and V_{cmax25} were nearly two

times those of R_{d25} and g_{m25}. Figure S2a shows a strong and significant positive relationship between the Morris μ and σ values.

To verify the effectiveness and reliability of the Morris method, we also used the Sobol' method to assess the key parameters in the FvCB model. Based on the thresholds in Tang et al. (2007a, b), we again found that J_{max25} and V_{cmax25} were the most sensitive parameters across all plant functional types (Fig. 2a). The average values of S_i ranged from 0.34 for DTS to 0.55 for NET for J_{max25} and from 0.19 for AGG to 0.28 for DTS for V_{cmax25} (Table S2). These values were about 10 times the values for the other parameters across all plant functional types. At the same time, the S_i values for R_{d25}, g_{m25}, K_{c25}, E_{J}, and α ranged between 0.01 and 0.1, indicating that these five parameters were sensitive and also affected the model outputs. The remaining parameters had S_i values less than 0.01, suggesting that these parameters were insensitive and that their variation had little effect on model simulations.
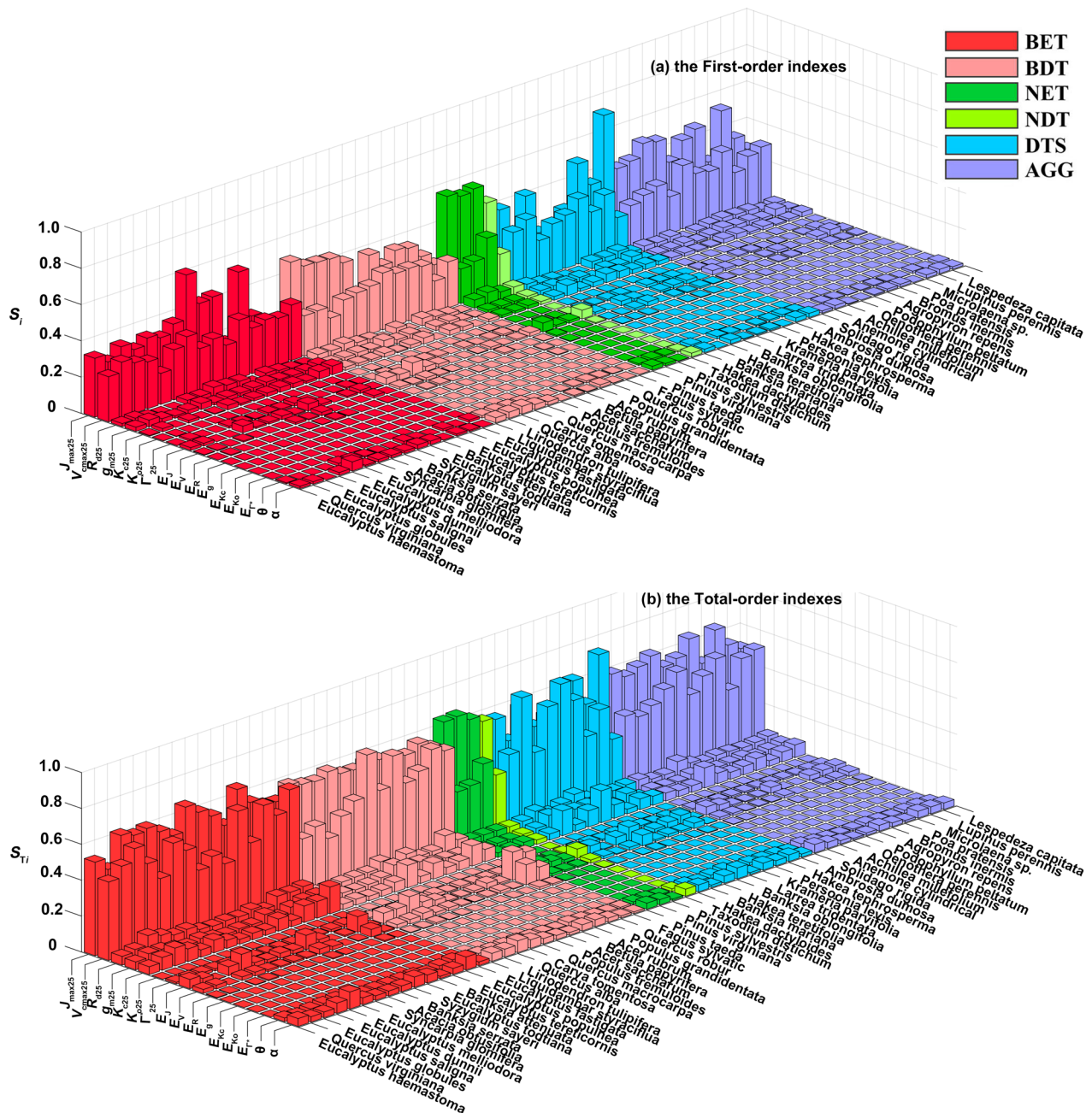
Figure 2b presents the results for the total-order sensitivity indexes (S_{Ti}). Once again, J_{max25} and V_{cmax25} were the most sensitive across all plant functional types, with S_{Ti} values ranging from 0.53 for DTS to 0.64 for NET for J_{max25} and from 0.31 for NDT to 0.49 for DTS for V_{cmax25}. J_{max25} contributed more than half of the total variance and V_{cmax25} contributed more than about one-third. The S_{Ti} values of E_{V} and θ were greater than 0.01, whereas their S_i values were smaller than 0.01. This suggested that although these parameters themselves had only a small effect, their interactions with other parameters had a noticeable effect on the model outputs. Overall, nine sensitive parameters

Table 3 Sensitivities of the 9 sensitive or highly sensitive parameters based on the mean (μ) elementary effect |EE|, and the resulting rankings for the size plant functional types (PFTs)

Parameter	BET		BDT		NET		NDT		DTS		AGG	
	μ	Rank	μ	Rank	μ	Rank	μ	Rank	μ	Rank	μ	Rank
J_{max25}	9.72	2	14.69	1	16.10	2	10.98	2	14.36	1	14.72	1
V_{cmax25}	10.12	1	11.83	2	20.61	1	23.13	1	10.91	2	10.02	2
R_{d25}	5.71	4	6.07	4	6.70	3	7.19	3	5.14	3	6.08	4
g_{m25}	6.55	3	8.61	3	6.42	4	5.42	4	4.18	4	7.87	3
K_{c25}	3.73	5	3.92	6	4.34	5	4.44	5	3.79	5	3.26	6
E_{J}	2.51	8	5.86	5	2.23	9	3.68	7	3.14	7	4.41	5
E_{V}	2.26	9	2.83	8	2.72	7	4.12	6	1.93	8	1.63	9
θ	2.63	7	2.7	9	2.77	6	1.64	8	1.92	9	2.15	8
α	2.90	6	3.60	7	2.69	8	1.40	9	3.41	6	3.09	7

PFTs: *AGG* agriculture/C3 grassland, *BDT* broadleaf-deciduous trees, *BET* broadleaf-evergreen trees, *DTS* dwarf trees and shrubs, *NDT* needleleaf-deciduous trees, *NET* needleleaf-evergreen trees. μ mean of |EE|

Parameters: E_{J} enthalpy of activation for J_{max}, E_{V} enthalpy of activation for V_{cmax}, g_{m25} mesophyll conductance, J_{max25} light-saturated electron transport rate at 25 °C, K_{c25} Michaelis–Menten constant at 25 °C, R_{d25} dark respiration in the light at 25 °C, V_{cmax25} maximum carboxylation rate of Rubisco at 25 °C, α leaf absorbance, θ light-response curvature
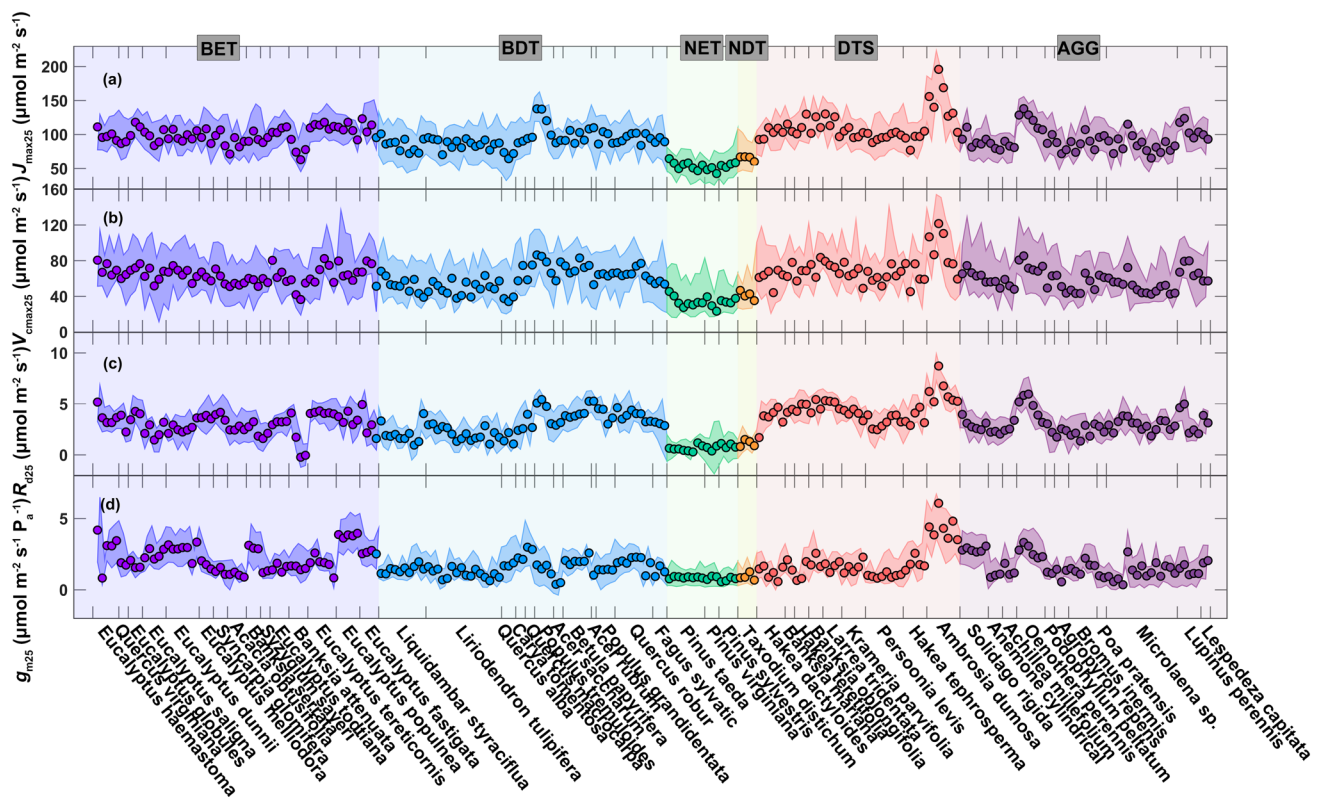
Fig. 2 The **a** first-order (S_i) and **b** total-order (S_{Ti}) sensitivity indexes for the 16 parameters in the 51 species. Parameters: E_J enthalpy of activation for J_{max}, E_V enthalpy of activation for V_{cmax}, E_R enthalpy of activation for R_d, E_g enthalpy of activation for g_m, E_{Kc} enthalpy of activation for K_c, E_{Ko} enthalpy of activation for K_o, $E_{\Gamma*}$ enthalpy of activation for $\Gamma*$, g_{m25} mesophyll conductance, J_{max25} light-saturated electron transport rate at 25 °C, K_{c25} Michaelis–Menten constant at 25 °C, K_{o25} Michaelis–Menten constant for Rubisco at 25 °C, R_{d25} dark respiration in the light at 25 °C, V_{cmax25} maximum carboxylation rate of Rubisco at 25 °C, α leaf absorbance, Γ_{25}^* CO_2 compensation point when mitochondrial respiration is zero at 25 °C, θ light-response curvature

(J_{max25}, V_{cmax25}, R_{d25}, g_{m25}, K_{c25}, E_J, E_V, θ, and α) contributed strongly to the model outputs across plant functional types, whereas the remaining seven insensitive parameters had almost negligible effects. We observed similar results when we used the *NSE* and *Bias* goodness-of-fit metrics (see Supplementary Material Figs. S1g–r, S3, and S4).

Hierarchical Bayesian parameterization

Figures 3 and 4 show the plant-level posterior distributions for the highly sensitive and sensitive parameters. The hierarchical Bayesian algorithm was generally able to decrease the ranges of the prior distributions of the parameters, as
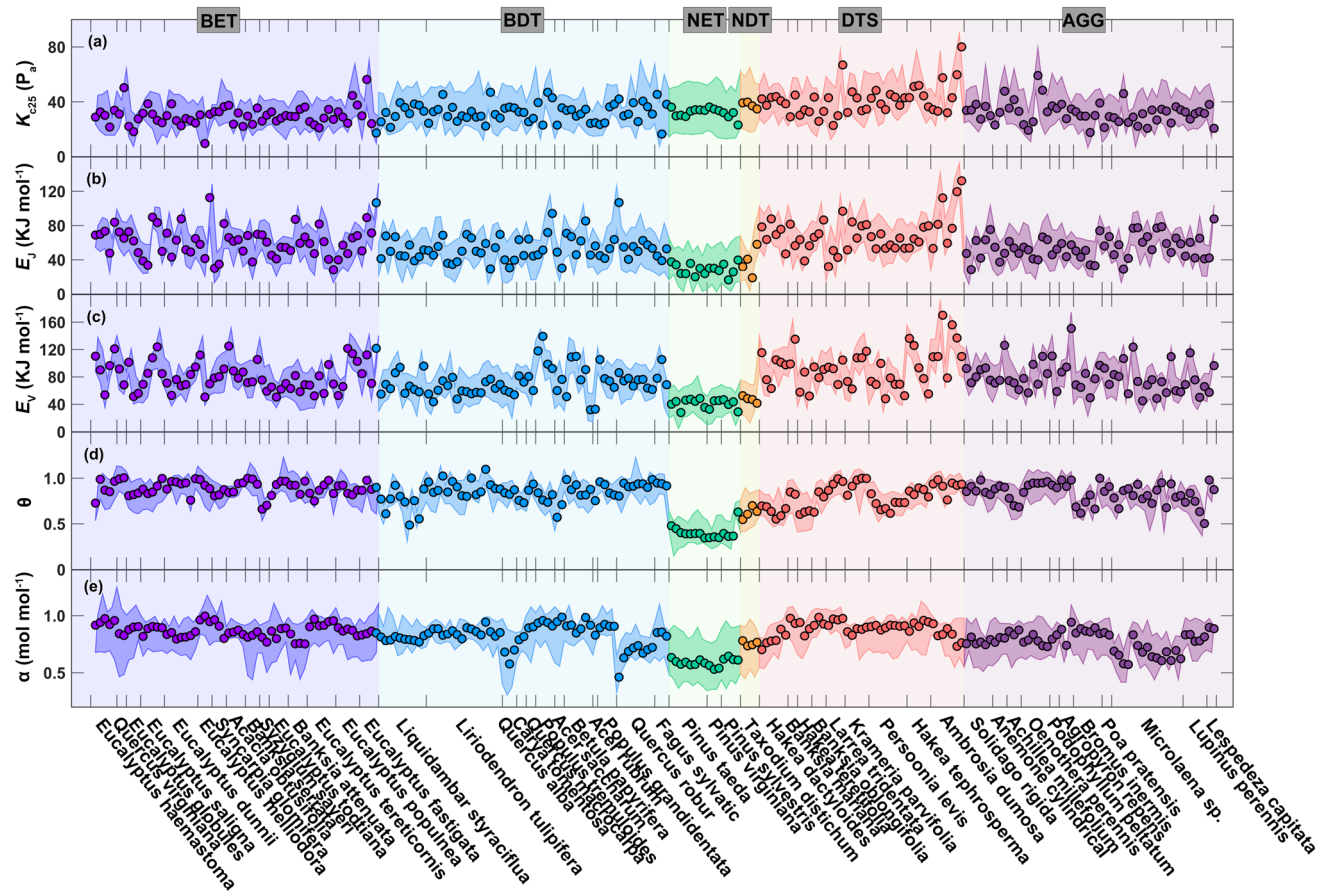
Fig. 3 Posterior medians (filled circles) and 95% confidence intervals (CI, shaded areas) for plant-level variation estimated using the hierarchical Bayesian framework based on 236 curves for the relationship between net CO_2 assimilation and changes in the intercellular CO_2 concentration for the highly sensitive photosynthetic parameters. Estimates are shown for **a** the maximum electron transport rate at 25 °C (J_{max25}), **b** the maximum rate of Rubisco activity at 25 °C (V_{cmax25}), **c** the leaf dark respiration rate in the light at 25 °C (R_{d25}), and **d** mesophyll conductance at 25 °C (g_{m25}). Plant-level estimates were calculated for the six plant functional types (PFTs): *AGG* agriculture/C3 grassland, *BDT* broadleaf-deciduous trees, *BET* broadleaf-evergreen trees, *DTS* dwarf trees and shrubs, *NDT* needleleaf-deciduous trees, *NET* needleleaf-evergreen trees

shown by the relatively narrow 95% credible intervals (CIs). All nine highly sensitive or sensitive parameters (i.e., J_{max25}, V_{cmax25}, R_{d25}, g_{m25}, K_{c25}, E_J, E_V, θ, and α) exhibited plant-level variation (Figs. 3, 4; Table S3). J_{max25} and V_{cmax25} varied from 42.61 to 205.90 μmol m^{-2} s^{-1} and from 23.53 to 121.70 μmol m^{-2} s^{-1}, respectively. Both parameters generally had smaller posterior medians for needle-leaved trees than for the other plant functional types (Fig. 3). Moreover, the posterior medians of J_{max25} and V_{cmax25} were significantly positively correlated ($P < 0.01$, $n = 236$; Fig. 5a) without imposing restrictions on prior information between the two parameters. Among different plant functional types, the standard major axis (SMA) slopes of J_{max25} and V_{cmax25} ranged from 1.71 (95% CI 1.51, 1.94) for AGG to 2.37 (95% CI 1.93, 2.92) for NET (further details about slopes and intercepts with 95% CI, coefficients of determination (R^2), P value, and sample size for each plant functional types were given in Table S4). The plant-level posterior medians for R_{d25} ranged from 0.29 μmol m^{-2} s^{-1} to 8.73 μmol m^{-2} s^{-1} across all plants, except for two outliers (with values of -0.23 and -0.04 μmol m^{-2} s^{-1} for two plans named

Banksia attenuata). R_{d25} was also positively correlated with V_{cmax25} across plants ($P < 0.01$, $n = 236$; Fig. 5b). The SMA slopes of R_{d25} and V_{cmax25} ranged from 0.07 to 0.11 among plant functional types, and exhibited no significant difference (further details about slopes and intercepts with 95% CI were provided in Table S4). In addition, g_{m25} varied widely among the plants, with a minimum value of 0.36 μmol m^{-2} s^{-1} P$_a^{-1}$ and a maximum value of 6.07 μmol m^{-2} s^{-1} P$_a^{-1}$ (Fig. 3d). K_{c25}, E_J, E_V, θ, and α, which were previously assumed to be constant across species (von Caemmerer 2000; Bernacchi et al. 2001), exhibited considerable variation (Fig. 4; Table S3).

Figure 6 shows the posterior medians at the species level. For J_{max25}, the median ranged from 52.82 μmol m^{-2} s^{-1} (*Pinus virginiana*) to 138.80 μmol m^{-2} s^{-1} (*Ambrosia dumosa*), and V_{cmax25} ranged from 35.04 μmol m^{-2} s^{-1} (*Pinus sylvestris*) to 82.00 μmol m^{-2} s^{-1} (*Ambrosia dumosa*). R_{d25} at the species level ranged from 0.45 μmol m^{-2} s^{-1} (*Pinus sylvestris*) to 4.30 μmol m^{-2} s^{-1} (*Ambrosia dumosa*). The posterior distributions of J_{max25}, V_{cmax25}, and R_{d25} seemed much lower for needle-leaved species. The species-level
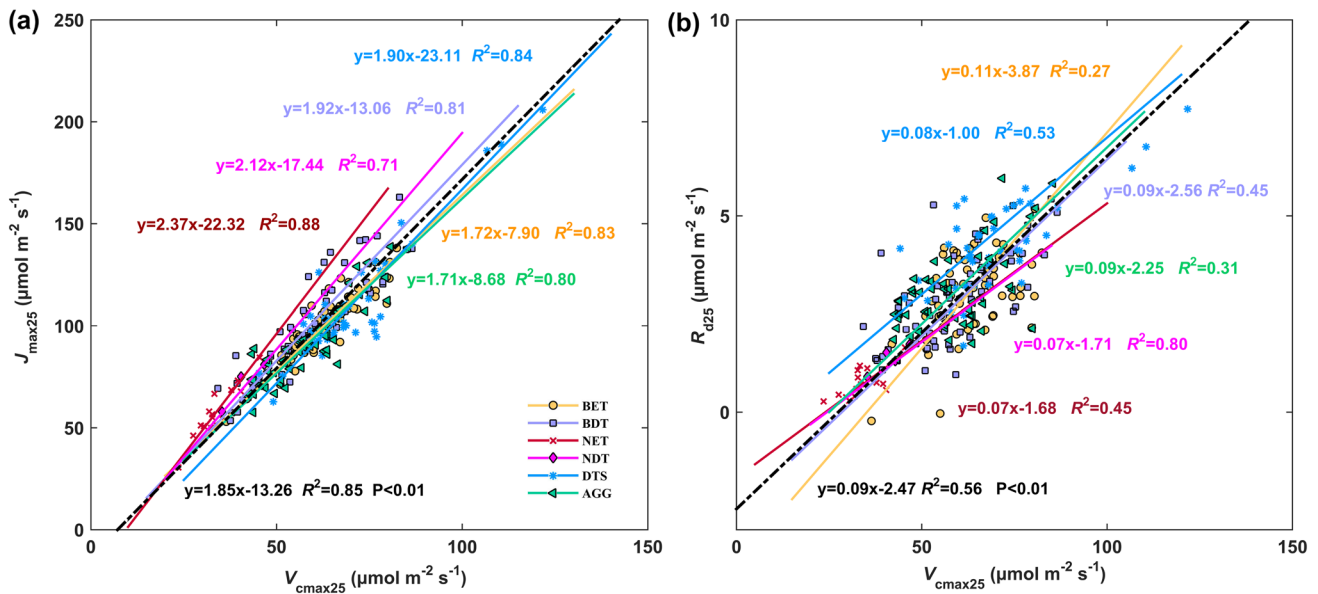
Fig. 4 Posterior medians (filled circles) and 95% confidence intervals (shaded areas) for plant-level variation using the hierarchical Bayesian framework based on 236 curves for the relationship between net CO_2 assimilation and changes in the intercellular CO_2 concentration for the sensitive photosynthetic parameters. Estimates are shown for **a** the Michaelis–Menten constant for carboxylation at 25 °C (K_{c25}), **b** the activation enthalpy for J_{max} (E_J), **c** the activation enthalpy for V_{cmax} (E_V), **d** light-response curvature (θ), and **e** leaf absorbance (α). Plant-level estimates were calculated for the six plant functional types (PFTs): *AGG* agriculture/C3 grassland, *BDT* broadleaf-deciduous trees, *BET* broadleaf-evergreen trees, *DTS* dwarf trees and shrubs, *NDT* needleleaf-deciduous trees, *NET* needleleaf-evergreen trees

posterior medians of g_{m25} exhibited wide variation, with the lowest value of 0.79 μmol m^{-2} s^{-1} P$_a^{-1}$ (*Acer saccharum*) and the highest of 4.04 μmol m^{-2} s^{-1} P$_a^{-1}$ (*Ambrosia dumosa*). K_{c25} showed slightly higher values for DTS species than for other species. E_J and E_V for needle-leaved (NET and NDT) species were obviously lower than for other species. Interestingly, the light-response curvature (θ) and leaf absorbance (α) varied widely, median of them from 0.41 to 0.99 for θ and from 0.58 to 0.99 mol mol^{-1} for α. Table S5 provides the medians and 95% CIs for all species at the species level.

At the level of the plant functional types, the values of the sensitive and highly sensitive parameters also exhibited obvious differences among plant functional types (Fig. 7). For example, J_{max25} values ranged from 54.71 for NET to 107.10 μmol m^{-2} s^{-1} for DTS and V_{cmax25} values ranged from 35.72 for NET to 75.30 μmol m^{-2} s^{-1} for DTS. At the level of the plant functional types, R_{d25} values ranged from 1.44 for NET to 3.64 μmol m^{-2} s^{-1} for DTS and g_{m25}

values ranged from 0.99 for NDT to 1.87 μmol m^{-2} s^{-1} P$_a^{-1}$ for DTS. The posterior distributions for J_{max25}, V_{cmax25}, and R_{d25} were generally highest for shrubs and herbaceous plants (DTS and AGG), intermediate for deciduous trees (BET and BDT), and lowest for needle-leaved trees (NET and NDT). g_{m25} values were lowest for needle-leaved trees (NET and NDT), but did not differ significantly among the other plant functional types. The posterior distributions for K_{c25} was significantly higher for DTS than for the other plant functional types. The two activation energy parameters had values that ranged from 30.10 (NET) to 66.74 kJ mol^{-1} (DTS) for E_J and from 41.91 (NET) to 90.99 kJ mol^{-1} (DTS) for E_V (Table 4). The posterior distributions of θ were significantly lower for the needle-leaved plant functional types (NET and NDT) and the posterior distributions of α was significantly lower for NET, with no significant differences among the other plant functional types.

Fig. 5 Relationships between the posterior medians of **a** the maximum electron transport rate at 25 °C (J_{max25}) and the maximum rate of Rubisco activity at 25 °C (V_{cmax25}) at the individual plant level; and **b** leaf dark respiration in the light at 25 °C (R_{d25}) and the maximum rate of Rubisco activity at 25 °C (V_{cmax25}) in using standard major axis (SMA) analyses with 95% confidence intervals (CIs) for different PFTs. PFTs: *AGG* agriculture/C3 grassland, *BDT* broadleaf-deciduous trees, *BET* broadleaf-evergreen trees, *DTS* dwarf trees and shrubs, *NDT* needleleaf-deciduous trees, *NET* needleleaf-evergreen trees

Figure S5 shows the posterior distributions for the seven insensitive parameters (E_R, E_g, E_{Kc}, E_{Ko}, $E_{\Gamma*}$, K_{o25}, and Γ_{25}^*), and Table S6 provides detailed statistics for these parameters. The shape of plots revealed that these insensitive parameters did not differ significantly among the plant functional types. The present medians were in excellent agreement with values derived from traditional research [63.90 kJ mol^{-1}, 49.6 kJ mol^{-1}, 70.40 kJ mol^{-1}, 29.80 kJ mol^{-1}, 26.80 kJ mol^{-1}, 16.58 kPa, and 3.74 Pa for E_R, E_g, E_{Kc}, E_{Ko}, $E_{\Gamma*}$, K_{o25}, and Γ_{25}^*, respectively; Sharkey et al. (2007)].
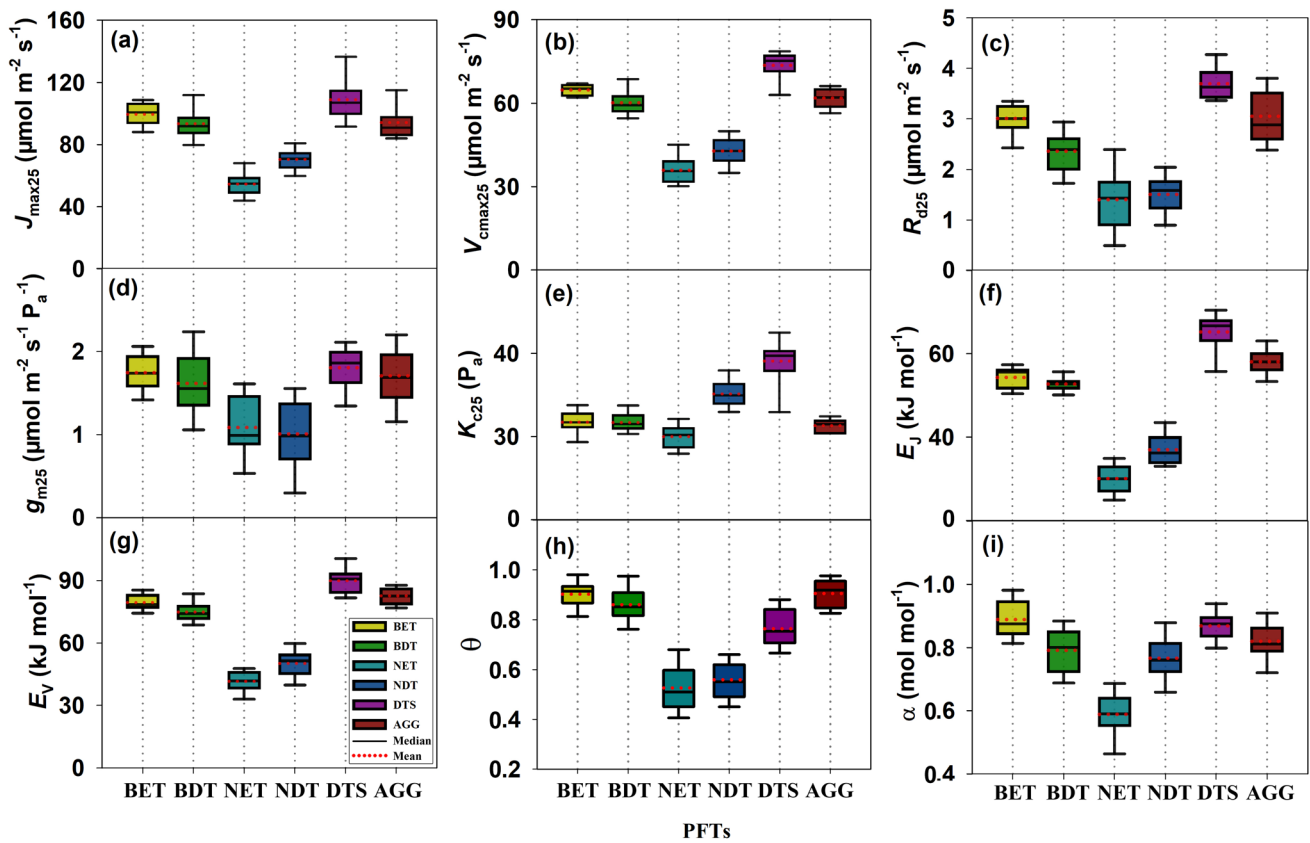
Performance of the FvCB model with parameters at different hierarchical levels

Having parameterized the FvCB model as described in the previous sections, we ran the model to simulate A_n (Eq. 1) using parameter values at the plant, species, and plant functional type levels. Figure 8 provides a scatterplot of the observed and simulated values of A_n. Table S7 provides the detailed regression results. Obviously, the FvCB model with plant-level parameters performed best. Points in the scatterplot for the observed-versus-simulated net photosynthetic rates fell close to the 1:1 line (Fig. 8a), with R^2 ranging from 0.97 to 0.99 and *RMSE* ranging from 0.40 to 1.31. Model performance using the species-level parameters was generally acceptable. *RMSE* ranged from 0.90 to 5.98, with R^2 ranging from 0.83 to 0.95, and the results were tightly

clustered around the 1:1 line (Fig. 8b). The simulations that used parameters at the level of plant functional types had the lowest accuracy, with R^2 ranging from 0.53 to 0.93 and *RMSE* ranging from 1.57 to 11.64.

Given that the FvCB model is based on a mechanistic model of photosynthesis, it's important to confirm that the values of the parameters estimated by the hierarchical Bayesian method were biochemically meaningful. We randomly selected six species (i.e., *Eucalyptus todtiana*, *Liquidambar styraciflua*, *Pinus taeda*, *Taxodium distichum*, *Persoonia levis*, and *Microlaena* sp.) which belonged to the BET, BDT, NET, NDT, DTS, and AGG plant functional types, respectively, to visualize the differences in model performance using parameters determined at the plant (Fig. 9a–f), species (Fig. 9g–l), and plant function type levels (Fig. 9m–r). In the FvCB model, the CO_2 assimilation rate is limited by either Rubisco or by regeneration of RuBP. (We omitted limitations caused by triose phosphate use in our analysis because, as noted in the Methods section, this is generally not a large factor.) Obviously, both the Rubisco-limited stage (A_c) and the RuBP-limited stage (A_j) were fitted well when the FvCB model used plant-level parameters. However, the model's performance using parameter values at the species or plant function type levels decreased. For example, the A/C_i curve for *Taxodium distichum*, *Persoonia levis*, and *Microlaena* sp. using the plant functional type parameters showed that the RuBP-limited stage provided a best fit to the observed

Fig. 6 Posterior distributions of the highly sensitive and sensitive parameters for each species. Values are medians (horizontal lines) and the 95% confidence intervals (bars). Species-level estimates were divided into six plant functional types (PFTs): AGG, agriculture/C3 grassland; BDT, broadleaf-deciduous trees; BET, broadleaf-evergreen trees; DTS, dwarf trees and shrubs; NDT, needleleaf-deciduous trees; NET, needleleaf-evergreen trees. Parameters: E_J enthalpy of activation for J_{max}, E_V enthalpy of activation for V_{cmax}, g_{m25} mesophyll conductance, J_{max25} light-saturated electron transport rate at 25 °C, R_{d25} dark respiration in the light at 25 °C, V_{cmax25} maximum carboxylation rate of Rubisco at 25 °C, α leaf absorbance, θ light-response curvature

Fig. 7 Posterior distribution of the highly sensitive and sensitive parameters for each of the six plant functional types (PFTs): *AGG* agriculture/C3 grassland, *BDT* broadleaf-deciduous trees, *BET* broadleaf-evergreen trees, *DTS* dwarf trees and shrubs, *NDT* needle-leaf-deciduous trees, *NET* needleleaf-evergreen trees. The values are medians (horizontal lines) and 95% confidence intervals (vertical bars). Parameters: E_J enthalpy of activation for J_{max}, E_V enthalpy of activation for V_{cmax}, g_{m25} mesophyll conductance, J_{max25} light-saturated electron transport rate at 25 °C, R_{d25} dark respiration in the light at 25 °C, V_{cmax25} maximum carboxylation rate of Rubisco at 25 °C, α leaf absorbance, θ light-response curvature

data, despite the underlying presence of the Rubisco-limited stage (Fig. 9p-r).

Discussion

Sensitivity analysis results

The biochemically based FvCB model provides a robust mechanistic representation of photosynthesis, and has therefore become the foundation for estimating GPP in many land surface models (Bonan et al. 2011; Rogers et al. 2017). However, except for the errors caused by model structure and data quality, model parameters impose considerable error when using these photosynthetic parameters empirically (Wullschleger 1993; Bonan et al. 2002; Orr et al. 2016). Thus, much effort should devote to obtain optimal parameters for characterizing the photosynthetic heterogeneity of vegetation (Patrick et al. 2009). Therefore, identifying the sensitive parameters in the FvCB model and analyzing their

interactions is crucial for further optimization. Our sensitivity analysis showed that the net photosynthesis rate was highly sensitive or sensitive to 9 of the 16 parameters (J_{max25}, V_{cmax25}, R_{d25}, g_{m25}, K_{c25}, E_J, E_V, θ, and α) at plant functional types, species, or even individual plant level. Figure S1, S3, and S4 provide comparable results using the *NSE* and *Bias* goodness-of-fit results, suggesting that our approach is reliable.
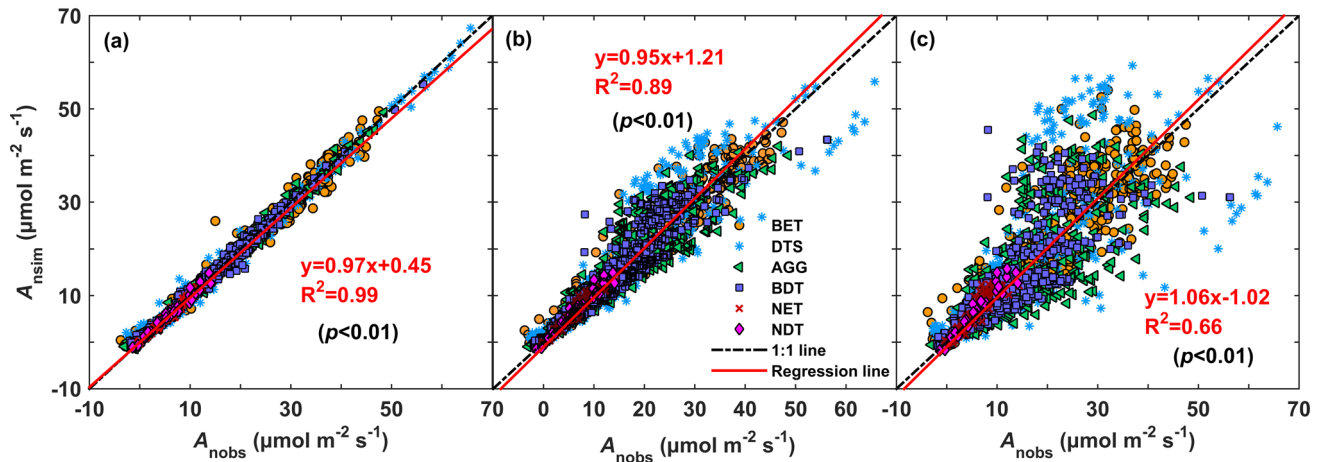
J_{max25} and V_{cmax25} were highly sensitive parameters across all plant functional types. As J_{max25} and V_{cmax25} limit the photosynthetic rate at high and low CO_2 concentrations, respectively, their values directly restrict RuBP-limited (A_j) and Rubisco-limited photosynthesis (A_c). Previous studies have confirmed that appropriate values of J_{max25} and V_{cmax25} were crucial to accurately estimate net photosynthesis rate (Wullschleger 1993; Feng and Dietze 2013; Brito et al. 2014; Atkin et al. 2015). After considering the seasonal variation of J_{max25} and V_{cmax25}, Zhu et al. (2011) provided a more accurate simulation of A_n in a typical desert riparian forest in northwestern China. Besides, R_{d25} was another parameter to

Table 4 Posterior probability distributions (medians and 95% credible intervals [CIs]) for highly sensitive and sensitive parameters at the level of the six plant functional types (PFTs)

Parameters	PFT					
	BET	BDT	NET	NDT	DTS	AGG
	Median [95% CI]	Median [95% CI]	Median [95% CI]	Median [95% CI]	Median [95% CI]	Median [95% CI]
J_{max25} (µmol m^{-2} s^{-1})	100.90 [84.83 109.90]	92.01 [85.41 194.21]	54.71 [42.94 70.07]	71.01 [60.25 81.30]	107.10 [91.05 117.20]	91.05 [83.77 105.90]
V_{cmax25} (µmol m^{-2} s^{-1})	65.30 [62.78 67.20]	59.40 [53.75 64.14]	35.72 [30.23 45.21]	42.94 [35.00 50.01]	75.30 [70.41 78.90]	62.13 [56.02 67.10]
R_{d25} (µmol m^{-2} s^{-1})	3.01 [2.22 3.47]	2.40 [1.67 2.95]	1.44 [0.50 2.40]	1.59 [0.89 2.06]	3.64 [3.36 4.30]	2.89 [2.38 3.85]
g_{m25} (µmol m^{-2} s^{-1} P$_a^{-1}$)	1.74 [1.94 2.88]	1.56 [0.99 2.31]	1.00 [0.50 1.63]	0.99 [0.30 1.56]	1.87 [1.32 2.12]	1.69 [1.13 2.23]
K_{c25} (P$_a$)	31.44 [28.46 30.81]	31.55 [30.00 34.41]	30.24 [28.00 32.17]	35.00 [33.00 38.01]	39.76 [37.56 42.73]	31.53 [20.46 32.47]
E_J (kJ mol^{-1})	55.73 [58.10 62.22]	52.84 [49.77 55.78]	30.10 [25.00 35.02]	36.31 [29.99 44.01]	66.74 [62.24 70.79]	58.13 [53.47 56.59]
E_V (kJ mol^{-1})	78.61 [73.89 86.67]	74.26 [67.74 85.95]	41.91 [32.00 48.01]	51.69 [40.00 87.17]	90.99 [81.79 101.40]	82.79 [75.92 85.97]
θ (dimensionless)	0.92 [0.81 0.98]	0.85 [0.76 0.99]	0.51 [0.41 0.68]	0.55 [0.45 0.66]	0.76 [0.66 0.88]	0.92 [0.83 0.99]
α (mol mol^{-1})	0.88 [0.79 0.98]	0.80 [0.68 0.89]	0.59 [0.46 0.69]	0.76 [0.66 0.88]	0.88 [0.80 0.94]	0.82 [0.69 0.93]

PFTs: *AGG* agriculture/C3 grassland, *BDT* broadleaf-deciduous trees, *BET* broadleaf-evergreen trees, *DTS* dwarf trees and shrubs, *NDT* needleleaf-deciduous trees, *NET* needleleaf-evergreen trees
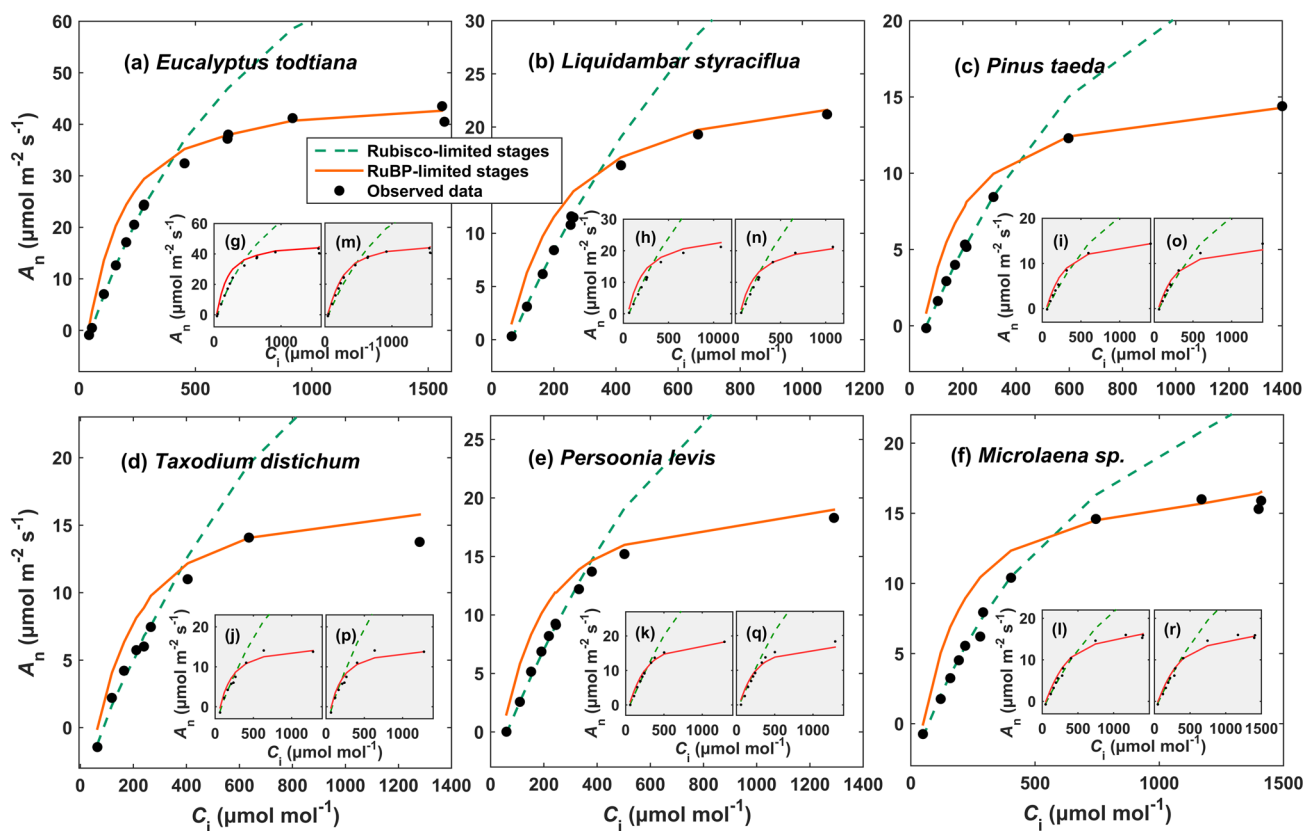
Parameters: E_J enthalpy of activation for J_{max}, E_V enthalpy of activation for V_{cmax}, E_R enthalpy of activation for R_d, E_g enthalpy of activation for g_m, E_{Kc} enthalpy of activation for K_c, E_{Ko} enthalpy of activation for K_o, $E_{\Gamma*}$ enthalpy of activation for Γ^*, g_{m25} mesophyll conductance, J_{max25} light-saturated electron transport rate at 25 °C, K_{c25} Michaelis–Menten constant at 25 °C, K_{o25} Michaelis–Menten constant for Rubisco at 25 °C, R_{d25} dark respiration in the light at 25 °C, V_{cmax25} maximum carboxylation rate of Rubisco at 25 °C, α leaf absorbance, Γ_{25}^* CO$_2$ compensation point when mitochondrial respiration is zero at 25 °C, θ light-response curvature

Fig. 8 Regression between the observed (A-$_{nobs}$) and simulated (A_{nsim}) net photosynthetic rates. Regressions were conducted using the derived parameter values at the **a** plant level, **b** species level and **c** plant functional type (PFT) level. The DIC was used for model selection (DIC$_{(a)}$ = 973.44, DIC$_{(b)}$ = 633.52, and DIC$_{(c)}$ = 1583.68). PFTs: *AGG* agriculture/C3 grassland, *BDT* broadleaf-deciduous trees, *BET* broadleaf-evergreen trees, *DTS* dwarf trees and shrubs, *NDT* needleleaf-deciduous trees, *NET* needleleaf-evergreen trees

Fig. 9 Relationships between the simulated curve for the net photosynthetic rate (A_n) and the intercellular CO_2 concentration (C_i) for six representative species from different plant functional types (PFTs): **a** *Eucalyptus todtiana* (broadleaf-evergreen trees), **b** *Liquidambar styraciflua* (broadleaf-deciduous trees), **c** *Pinus taeda* (needleleaf-ever-green trees), **d** *Taxodium distichum* (needleleaf-deciduous trees), **e** *Persoonia levis* (dwarf trees and shrubs), and **f** *Microlaena* sp. (agri-culture/C3 grassland) at the plant (**a–f**), species (**g–l**), and plant functional type levels (**m–r**)

which A_n was sensitive. This parameter can reveal CO_2 evolution from mitochondria under lighted conditions, which is a significant process of the carbon lost by plants, and is central to the prediction of plant photosynthesis capacity with the FvCB model. Furthermore, g_{m25} were also identified as sensitive parameter in our study. It is important because stomatal aperture dominates a plant's photosynthesis process and responds rapidly to changes in environmental conditions such as the air temperature, relative humidity, and soil water content (Lin et al. 2015; Franks et al. 2018).

Interestingly, parameters K_{c25}, E_J, E_V, θ, and α, which were paid relatively less attention in model simulation, were found to be sensitive to model output. K_{c25} describes intrinsic properties of Rubisco which tendency to confuse the photosynthetic substrate (CO_2) with the product (O_2), and determines the efficiency with which plants use their basic resources of light, water, and N (Tcherkez et al. 2006; Orr et al. 2016). The Rubisco-limited stage of photosynthesis (A_c) can be restricted by the parameter K_{c25}. Therefore, the variation of K_{c25} would have a big influence on the photosynthetic rates simulation. In terms of the model structure,

E_J and E_V represent the exponential rate of increase of the Arrhenius function. Fluctuations of both parameters are directly linked with the accuracy of simulations of J_{max} and V_{cmax}. At the same time, the activation energy, E_J and E_V, is a measure of temperature dependence of A_j and A_c, respectively (Yamori et al. 2005). Previous study has confirmed that the optimal temperature of A_j and A_c was influenced by the variation of E_J and E_V (Hikosaka et al. 2006). That may be why optimal values of E_J and E_V significantly improved estimates of A_n. θ and α are related to the underlying optical properties of a leaf, which were believed to be similar across diverse C_3 species with empirical values of around 0.7 and 0.85 (Evans 1989; Kosugi et al. 2003). In the present study, the magnitude of the effect of parameter interactions on sensitivity (i.e., $S_{Ti} - S_i$) accounted for an important proportion of their total-order indexes. Such results suggest that θ and α can affect model performance through their interactions with other parameters. Furthermore, Ögren and Evans (1993) found that plants had high CO_2 assimilation rate commonly with low θ values, while plants had low CO_2 assimilation rate with high θ values. Therefore, to simulate

a more reliable A_n, more accurate values of these sensitive parameters are required.

Parameterization of the hierarchical Bayesian model

Given that the FvCB model has been widely used as the basis for predicting carbon assimilation across a diverse range of PFTs, it is important to understand how the underlying behavior of the biochemical parameters varies among plant functional types, species, or individual plants. Our results provide new insights into these parameters based on a combination of sensitivity analysis and the hierarchical Bayesian framework based on 236 A/C_i curves from across continents and species. In particular, when comparing our results with the results based on the simple Bayesian framework, we found that the model in using hierarchical Bayesian framework exhibited a much better performance (*RMSE* values were 5.56 and 1.08, and the DIC values were 1755.81 and 973.44 based on the simple Bayesian and hierarchical Bayesian framework, respectively; Figure S6; Table S8).

Parameter J_{max25}, V_{cmax25}, R_{d25}, and g_{m25} exhibited obvious variability at the levels of plants, species, and plant functional types (Figs. 3, 6 and 7; Table S3). The posterior medians generally fell within the range of values reported in previous research (Wullschleger 1993; Zhu et al. 2011). Furthermore, J_{max25} and V_{cmax25} demonstrated much lower values for needle-leaved trees (NET and NDT) than for other plant functional types (BET, BDT, DTS, and AGG). Medlyn and Dreyer (2002) observed similar results: J_{max25} ranged from 70.77 μmol m^{-2} s^{-1} for the needle-leaved tree *Pinus sylvestris* to 217.88 μmol m^{-2} s^{-1} for the agricultural species *Glycine max*. V_{cmax25} ranged from 41.64 μmol m^{-2} s^{-1} for *Abies alba* to 97.76 μmol m^{-2} s^{-1} for *Glycine max*. J_{max25} and V_{cmax25} have long been found to be correlated, with slopes ranging from 1.0 to 3.0 across species (Wullschleger 1993; Kattge and Knorr 2007; Miao et al. 2009). The SMA slopes of J_{max25} to V_{cmax25} in our study ranged from 1.71 to 2.37 with an average of 1.85 (Fig. 5a; Table S4), and heterogeneity were not significant among plant functional types. As has long been discussed, R_{d25} is not yet well understood, and hence, it has been difficult to estimate accurately (Way and Yamori 2014). As a result, researchers have commonly used a fixed relationship between R_{d25} and V_{cmax25} in their models (Bonan et al. 2011). Unfortunately, the relationship between R_{d25} and V_{cmax25} was not always constant among plant functional types (Fig. 5b), which was also confirmed by de Kauwe et al. (2016). Here, we found that the values of R_{d25} were generally highest for shrubs and herbaceous plants (DTS and AGG), intermediate for deciduous trees (BET and BDT) and lowest for needle-leaved trees (NET and NDT). Atkin et al. (2015) also found that R_{d25} values were higher in herbaceous plants (including C$_3$ herbs/grasses) than in trees (including broad-leaved trees and needle-leaved trees)

based on an analysis of 899 species. Our findings therefore improve estimates of R_{d25} in the FvCB model and will improve associated estimates of carbon cycle components in land surface models. Extensive work has been done to compare g_m values among species or plant functional types (Brito et al. 2014). For instance, Flexas et al. (2008) argued that herbaceous plants had the largest g_m values (ca. 4 mol μmol m^{-2} s^{-1} P$_a^{-1}$), followed by deciduous trees (*c.* 2 μmol m^{-2} s^{-1} P$_a^{-1}$), whereas evergreen trees had the lowest g_m values (around 1 μmol m^{-2} s^{-1} P$_a^{-1}$). However, there are also limitations in our understanding of g_m at 25 °C (g_{m25}) that may lead to biases in using empirical values, which have mostly been based on limited data for tobacco plants (Walker et al. 2013). In the present study, the values of g_{m25} showed no obvious differences among BET, BDT, DTS, and AGG, but the values for needle-leaved trees (NET and NDT) were much lower, with average values of around 1.01 μmol m^{-2} s^{-1} P$_a^{-1}$; this agrees with the results of Flexas et al. (2008). This difference may be driven by the unique leaf structural characteristics of needle-leaved trees, which have thicker cell walls and lower ratio of exposed chloroplast surface to leaf area (Tomás et al. 2013).

Originally, the use of Michaelis–Menten constant for carboxylation (K_{c25}) was conserved, whose value was around 27.24 Pa for most C$_3$ plants (von Caemmerer 2000). However, there is mounting evidence that K_{c25} is not constant. A recent study revealed significant variation in K_{c25} across 75 species that resulted from diversity of the catalytic function in Rubisco (Orr et al. 2016). Variations were also confirmed in our study, with higher posterior distributions for K_{c25} in DTS than in the other plant functional types. This emphasizes the need for additional work to improve our understanding of K_{c25}. Many current models related to the FvCB model assumed that E_J and E_V were constant and could be based on values that usually come from spinach (Jordan and Ögren 1984) or tobacco (Bernacchi et al. 2001). However, our results suggest that this assumption is not robust. For example, the values of E_J and E_V for needle-leaved trees (31.0 and 44.44 kJ mol^{-1} on average, respectively) were much lower than those of broad-leaved plants (58.36 and 80.73 kJ mol^{-1} on average, respectively). Thus, variation of E_J and E_V should be taken into account when using these parameters in future research. Until the present study, θ and α have been commonly assumed to be constant at 0.7 (Evans 1989) and 0.85 (von Caemmerer 2000), respectively. However, our results show that θ and α were both variable, with values of θ ranging from 0.41 for *Pinus taeda* to 0.99 for *Populus tremuloides* and with values of α ranging from 0.58 for *Pinus virginiana* to 0.99 for *Oenothera perennis*. These findings highlight the need to improve our understanding of these parameters both through better parameter estimation methods and from more accurate field gas-exchange data. All in all, the variation of parameters K_{c25}, E_J, E_V, θ, and

α at different levels confirmed our hypotheses that parameters commonly used as constant values in previous studies are evolvable within and/or across diverse species and plant functional types.

The FvCB model has been widely applied to scale photosynthesis from the leaf level to whole canopies or even biomes (Rogers et al. 2017). In most LSMs, some photosynthetic parameters are empirical values, whereas some are chosen at a coarse resolution to distinguish among plant functional types (Wullschleger et al. 2014; Fisher et al. 2015). However, the present results demonstrate that variations of parameters at the plant and species levels were significant (Figs. 3, 4, 6; Table S3). We also found that models based on plant- and species-level parameters performed much better fitting precision than models based on plant functional type parameters (Fig. 8, Tables S4, S7). These findings highlight the importance of considering species- and plant-level variation in sensitive parameters when applying these parameters in land surface models. Moreover, balancing model performance and model complexity is also very important in LSMs' simulation. The differences in DIC among the model in which parameters were used at different levels suggested that calibrating J_{max25}, V_{cmax25}, R_{d25}, g_{m25}, θ and α at species level, and K_{c25}, E_J, and E_V at plant functional types level was more reasonable than directly using a fixed value or at other levels, although these parameters exhibited obvious variability at the three levels simultaneously (further details were provided in the Supplementary Material Table S8). In summary, combining sensitivity analysis with a hierarchical Bayesian approach provided an effective framework to identify and optimize parameters in the FvCB model across a diverse range of species. The results not only improved our understanding of the behavior of these parameters, but also provided more accurate estimates of the parameter values for use in land surface models to simulate the carbon cycle.

Looking forward

For the moment, working at the resolution of the PFTs offers a reasonable compromise, as this level has been well integrated into LSMs [SiB2 (Sellers et al. 1995a, b); CLM4.5 (Oleson et al. 2013)]. Most current models use PFT-specific constant parameter values for regional or global applications (Wullschleger et al. 2014), and do not account for species- and plant-level variation. Our results demonstrated that variation of parameters at the species and plant levels was also highly significant, and should be considered in future models. Also, some field experiments documented that the variation of plant traits in species level was large and often even greater than that in plant functional types level (Wright et al. 2005; Laughlin et al. 2010). Given recent advances in our ability, like the HB method, to model diverse variation in different levels (e.g., plant functional types and species), future research should present a more accurate parameterization scheme for LSMs.

Conclusions

To obtain more accurate values of the common key parameters used in the FvCB model and analyze their variation within and across different hierarchical levels (plant, species, and plant functional types), we combined the use of two sensitivity analysis methods (the Morris and Sobol' methods) and the hierarchical Bayesian parameter estimation method. The results were more accurate than the results of simulations with a simple Bayesian framework. We found that: (1) J_{max25} and V_{cmax25} were highly sensitive parameters and R_{d25}, g_{m25}, K_{c25}, E_J, E_V, θ, and α were sensitive parameters; thus, these parameters should be estimated as accurately as possible for each model; (2) J_{max25}, V_{cmax25}, and R_{d25} exhibited lower posterior distributions for needle-leaved trees (NET and NDT) than for the other plant functional types (BET, BDT, DTS, and AGG); thus, these parameters should be estimated separately for these groups; (3) the posterior medians of J_{max25} and V_{cmax25} were strongly correlated, suggesting that more work will be necessary to understand their relationship; and (4) variation of parameters at the species level should be accounted for in future research. Note that because our study focused on C_3 plants, the results should not be extended to C_4 plants. Such studies will further improve our understanding of the distributions of parameter values so that we can account for this variation in the photosynthesis modules of LSMs.

Compliance with ethical standards

Conflict of interest The authors declare that they have no conflicts of interest.

Ethical approval Our research complies with the ethical standards of our university and laboratory ethical standards.

References

Amane M (2011) Photosynthesis, grain yield, and nitrogen utilization in rice and wheat. Plant Physiol 155:125–129

Atkin OK, Bloomfield KJ, Reich PB, Tjoelker MG, Asner GP, Bonal D, Bönisch G, Bradford MG, Cernusak LA, Cosio EG, Creek D, Crous KY, Domingues TF, Dukes JS, Egerton JJG, Evans JR, Farquhar GD, Fyllas NM, Gauthier PPG, Gloor E, Gimeno TE, Griffin KL, Guerrieri R, Heskel MA, Huntingford C, Ishida FY, Kattge J, Lambers H, Liddell MJ, Lloyd J, Lusk CH, Martin RE, Maksimov AP, Maximov TC, Malhi Y, Medlyn BE, Patrick M, Mercado LM, Mirotchnick N, Ng D, Niinemets Ü, O'Sullivan OS, Phillips OL, Lourens P, Pieter P, Prentice IC, Salinas N, Rowland LM, Ryan MG, Stephen S, Martijn S, Nicholas GS, Turnbull MH, Mark C, Vander W, Fernando V, Veneklaas EJ, Weerasinghe LK, Wirth C, Wright IJ, Wythers KR, Xiang J, Xiang S, Zaragoza-Castells J (2015) Global variability in leaf respiration in relation to climate, plant functional types and leaf traits. New Phytol 206:614–636

Baly ECC (1935) The kinetics of photosynthesis. Proc R Soc Lond Ser B 117:218–239

Bernacchi CJ, Singsaas EL, Pimentel C, Portis Jr AR, Long SP (2001) Improved temperature response functions for models of Rubisco-limited photosynthesis. Plant Cell Environ 24:253–259

Bernacchi CJ, Portis AR, Nakano H, von Caemmerer S, Long SP (2002) Temperature response of mesophyll conductance. Implications for the determination of Rubisco enzyme kinetics and for limitations to photosynthesis in vivo. Plant Physiol 130:1–7

Blackman FF (1905) Optima and limiting factors. Ann Bot 19:281–295

Bonan GB, Oleson KW, Vertenstein M, Levis S (2002) The land surface climatology of the Community Land Model coupled to the NCAR Community Climate Model. J Clim 15:3123–3149

Bonan GB, Lawrence PJ, Oleson KW, Levis S, Jung M, Reichstein M, Lawrence DM, Swenson SC (2011) Improving canopy processes in the Community Land Model version 4 (CLM4) using global flux fields empirically inferred from FLUXNET data. J Geophys Res 116:G02014. https://doi.org/10.1029/2010JG001593

Brito C, Bown H, Fuentes J, Franck N, Perez-Quezada J (2014) Mesophyll conductance constrains photosynthesis in three common sclerophyllous species in Central Chile. Revista Chilena de Historia Natural 87:1–12

Campolongo F, Cariboni J, Saltelli A (2007) An effective screening design for sensitivity analysis of large models. Environ Model Softw 22:1509–1518

Carlin BP, Clark JS, Gelfand AE (2006) Elements of hierarchical Bayesian inference. In: Clark JS, Gelfand AE (eds) Hierarchical modelling for the environmental sciences: statistical methods and applications. Oxford University Press, New York, pp 3–24

Cibin R, Sudheer KP, Chaubey I (2010) Sensitivity and identifiability of stream flow generation parameters of the SWAT model. Hydrol Process 24:1133–1148

Clark JS (2005) Why environmental scientists are becoming Bayesians. Ecol Lett 8:2–14

Clark JS (2007) Models for ecological data: an introduction. Princeton University Press, Princeton

Collatz GJ, Ball JT, Grivet C, Berry JA (1991) Physiological and environmental regulation of stomatal conductance, photosynthesis, and transpiration: a model that includes a laminar boundary layer. Agric For Meteorol 54:107–136

De Kauwe MG, Lin YS, Wright IJ, Medlyn BE, Crous KY, Ellsworth DS, Maire V, Prentice IC, Atkin OK, Rogers A, Niinemets Ü, Serbin SP, Patrick M, Johan U, Togashi HF, Tarvainen L, Weerasinghe LK, Evans BJ, Ishida FY, Domingues TF (2016) A test of the 'one-point method' for estimating maximum carboxylation capacity from field-measured, light-saturated photosynthesis. New Phytol 210:1130–1144

Dubois JJB, Fiscus EL, Booker FL, Flowers MD, Reid CD (2007) Optimizing the statistical estimation of the parameters of the Farquhar–von Caemmerer-Berry model of photosynthesis. New Phytol 176:402–414

Ellsworth DS, Crous KY, Lambers H, Cooke J (2015) Phosphorus recycling in photorespiration maintains high photosynthetic capacity in woody species. Plant Cell Environ 38:1142–1156

Ethier GJ, Livingston NJ (2004) On the need to incorporate sensitivity to CO_2 transfer conductance into the Farquhar-von Caemmerer-Berry leaf photosynthesis mode. Plant Cell Environ 27:137–153

Evans JR (1987) The dependence of quantum yield on wavelength and growth irradiance. Aust J Plant Physiol 14:69–79

Evans JR (1989) Photosynthesis and nitrogen relationships in leaves of C3 plants. Oecologia 78:9–19

Farquhar GD, von Caemmerer S, Berry JA (1980) A biochemical model of photosynthetic CO_2 assimilation in leaves of C_3 species. Planta 149:78–90

Feng XH, Dietze M (2013) Scale dependence in the effects of leaf ecophysiological traits on photosynthesis: bayesian parameterization of photosynthesis models. New Phytol 4:1132–1144

Fischer RA, Byerlee D, Edmeades GO (2014) Crop yields and global food security: will yield increase continue to feed the world?. Australian Centre for International Agricultural Research, Canberra

Fisher JB, Huntzinger DN, Schwalm CR, Sitch S (2014) Modeling the terrestrial biosphere. Annu Rev Environ Resour 39:91–123

Fisher RA, Muszala S, Verteinstein M, Lawrence P, Xu C, McDowell NG, Knox RG, Koven C, Holm J, Rogers BM, Spessa A, Lawrence D, Bonan G (2015) Taking off the training wheels: the properties of a dynamic vegetation model without climate envelopes, CLM4.5 (ED). Geosci Model Dev 8:3593–3619

Flexas J, Ribas-Carbo M, Diaz-Espejo A, Galmes J, Medrano H (2008) Mesophyll conductance to CO_2: current knowledge and future prospects. Plant Cell Environ 31:602–612

Fox A, Williams M, Richardson AD, Camerond D, Govee GH, Quaifef T, Daniel R, Reichstein M, Tomelleri E, Trudinger CM, Van Wijk MT (2009) The REFLEX project: comparing different algorithms and implementations for the inversion of a terrestrial ecosystem model against eddy covariance data. Agric For Meteorol 149:1597–1615

Franks PJ, Bonan GB, Berry JA, Lombardozzi DL, Holbrook NM, Herold N, Oleson KW (2018) Comparing optimal and empirical stomatal conductance models for application in Earth system models. Glob Change Biol 24:5708–5723

Fu G, Butler D, Khu ST, Sun SA (2011) Imprecise probabilistic evaluation of sewer flooding in urban drainage systems using random set theory. Water Resour Res 47:1–13

Galmés J, Kapralov MV, Andralojc PJ, Conesa MA, Keys AJ, Parry MAJ, Flexas J (2014) Expanding knowledge of the Rubisco kinetics variability in plant species: environmental and evolutionary trends. Plant Cell Environ 37:1989–2001

Gálvez ED, Capuz-Rizo SF (2016) Assessment of global sensitivity analysis methods for project scheduling. Comput Ind Eng 93:110–120

Gelman A (2004) Parameterization and Bayesian modeling. J Am Stat Assoc 99:537–545

Gelman A (2006) Prior distributions for variance parameters in hierarchical models. Bayesian Anal 1:515–533

Hall JW, Tarantola S, Bates PD, Horritt MS (2005) Distributed sensitivity analysis of flood inundation model calibration. J Hydraul Eng 131:117–126

Han F, Zheng Y (2016) Multiple-response Bayesian calibration of watershed water quality models with significant input and model structure errors. Adv Water Resour 88:109–123

Hansen J, Nazarenko L, Ruedy R, Sato M, Willis J, Del Genio A, Koch D, Lacis A, Lo K, Menon S, Novakov T, Perlwitz J, Russell G, Schmidt GA, Tausnev N (2005) Earth's energy imbalance: confirmation and implications. Science 308:1431–1435

Harley PC, Sharkey TD (1991) An improved model of C_3 photosynthesis at high CO_2: reversed O_2 sensitivity explained by lack of glycerate reentry into the chloroplast. Photosynth Res 27:169–178

Harley PC, Tenhunen JD, Lange OL (1986) Use of an analytical model to study limitation on net photosynthesis in *Arbutus unedo* under field conditions. Oecologia 70:393–401

Harley PC, Thomas RB, Reynolds JF, Strain BR (1992) Modeling photosynthesis of cotton grown in elevated CO_2. Plant Cell Environ 15:271–282

Helton J, Davis F (2003) Latin hypercube sampling and the propagation of uncertainty in analyses of complex systems. Reliab Eng Syst Saf 81:23–69

Hermida-Carrera C, Kapralov MV, Galmés J (2016) Rubisco catalytic properties and temperature response in crops. Plant Physiol 171:2549–2561

Hikosaka K, Ishikawa K, Borjigidai A, Muller O, Onoda Y (2006) Temperature acclimation of photosynthesis: mechanisms involved in the changes in temperature dependence of photosynthetic rate. J Exp Bot 57:291–302

Jordan DB, Ögren WL (1984) The CO_2/O_2 specificity of ribulose 1,5-bisphosphate carboxylase/oxygenase. Dependence on ribulose bisphosphate concentration, pH and temperature. Planta 161:308–313

Kattge J, Knorr W (2007) Temperature acclimation in a biochemical model of photosynthesis: a reanalysis of data from 36 species. Plant Cell Environ 30:1176–1190

Kosugi Y, Shibata S, Kobashi S (2003) Parameterization of the CO_2 and H_2O gas exchange of several temperate deciduous broad-leaved trees at the leaf scale considering seasonal changes. Plant Cell Environ 26:285–301

Kucherenko S, Rodriguez-Fernandez M, Pantelides C, Shah N (2009) Monte Carlo evaluation of derivative-based global sensitivity measures. Reliab Eng Syst Saf 94:1135–1148

Laughlin DC, Leppert JJ, Moore MM, Sieg CH (2010) A multi-trait test of the leaf-height-seed plant strategy scheme with 133 species from a pine forest flora. Funct Ecol 24:493–501

Leuning R (1997) Scaling to a common temperature improves the correlation between the photosynthesis parameters J_{max} and V_{cmax}. J Exp Bot 48:345–347

Lin YS, Duursma RA, Prentice IC, Wang H, Baig S, Eamus D, de Dios VR, Wingate L (2015) Optimal stomatal behaviour around the world. Nat Clim Change 5:459–464

Lloyd J, Syvertsen JP, Kriedemann PE, Farquhar GD (1992) Low conductances for CO_2 diffusion from stomata to the sites of carboxylation in leaves of woody species. Plant Cell Environ 15:873–899

Long SP, Bernacchi CJ (2003) Gas exchange measurements, what can they tell us about the underlying limitations to photosynthesis? Procedures and sources of error. J Exp Bot 392:2393–2401

Luo YQ, White LW, Canadell JG, DeLucia EH, Ellsworth DS, Finzi A, Lichter J, Schlesinger WH (2003) Sustainability of terrestrial carbon sequestration: a case study in Duke Forest with inversion approach. Glob Biogeochem Cycles 17:1–13

McKay MD, Beckman RJ, Conover WJ (2000) A comparison of three methods for selecting values of input variables in the analysis of output from a computer code. Technometrics 42:55–61

Medlyn BE, Dreyer E (2002) Temperature response of parameters of a biochemically based model of photosynthesis. II. A review of experimental data. Plant Cell Environ 25:1167–1179

Medlyn BE, Duursma RA, Eamus D, Ellsworth DS, Prentice IC, Barton CVM, Crous KY, de Angelis P, Freeman M, Wingate L (2011) Reconciling the optimal and empirical approaches to modeling stomatal conductance. Glob Change Biol 17:2134–2144

Miao ZW, Xu M, Lathrop JR, Wang YF (2009) Comparison of the A-Cc curve fitting methods in determining maximum ribulose 1.5-bisphosphate carboxylase/oxygenase carboxylation rate, potential light saturated electron transport rate and leaf dark respiration. Plant Cell Environ 32:109–122

Michaelis L, Menten ML (1913) Die kinetik der invertinwirkung. Biochemische Zeitschrift 49:333–369

Morris MD (1991) Factorial sampling plans for preliminary computational experiments. Technometrics 33:161–174

Norros V, Laine M, Lignell R, Thingstad F (2017) Parameterization of aquatic ecosystem functioning and its natural variation: hierarchical Bayesian modelling of plankton food web dynamics. J Mar Syst 174:40–53

Nossent J, Elsen P, Bauwens W (2011) Sobol' sensitivity analysis of a complex environmental model. Environ Model Softw 26:1515–1525

Ögren E, Evans JR (1993) Photosynthetic light-response curves. I. The influence of CO_2 partial pressure and leaf inversion. Planta 189:182–190

Oleson K, Lawrence DM, Bonan GB, Drewniak B, Huang M, Koven CD, Levis S, Li F, Riley WJ, Subin ZM, Swenson S, Thornton PE, Bozbiyik A, Fisher R, Heald CL, Kluzek E, Lamarque JF, Lawrence PJ, Leung LR, Lipscomb W, Muszala SP, Ricciuto DM, Sacks WJ, Sun Y, Tang J, Yang ZL (2013) Technical description of version 4.5 of the Community Land Model (CLM). NCAR Technical Note NCAR/TN-503 + STR. https://doi.org/10.5065/d6rr1w7m

Orr DJ, Alcântara A, Kapralov MV, Andralojc PJ, Carmo-Silva E, Parry MAJ (2016) Surveying Rubisco diversity and temperature response to improve crop photosynthetic efficiency. Plant Physiol. https://doi.org/10.1104/00.16.00750

Patrick LD, Ogle K, Tissue DT (2009) A hierarchical Bayesian approach for estimation of photosynthetic parameters of C_3 plants. Plant Cell Environ 32:1695–1709

Pitman AJ (2003) The evolution of, and revolution in, land surface schemes designed for climate models. Int J Climatol 23:479–510

Qian T, Elings A, Dieleman JA, Gort G, Marcelis LFM (2012) Estimation of photosynthesis parameters for a modified Farquhar–von Caemmerer-Berry model using simultaneous estimation method and nonlinear mixed effects model. Environ Exp Bot 82:66–73

Rogers A, Medlyn BE, Dukes JS, Bonan G, von Caemmerer S, Dietze MC, Kattge J, Leakey ADB, Mercado LM, Niinemets Ü, Prentice IC, Serbin SP, Sitch S, Way DA, Zaehle S (2017) A roadmap for improving the representation of photosynthesis in Earth system models. New Phytol 213:22–42

Running SW, Hunt RE (1993) Generalization of a forest ecosystem process model for other biomes, BIOME-BGC, and an application for global-scale models. In: Ehleringer JR, Fields CB (eds) Scaling physiologic processes, leaf to globe. Academic Press, San Diego, pp 141–158

Sellers PJ, Los SO, Tucker CJ, Justice CO, Dazlich DA, Collatz GJ, Randall DA (1995a) A revised land surface parameterization (SiB2) for atmospheric GCMs. Part II: the generation of global fields of terrestrial biophysical parameters from satellite data. J Clim 9:706–736

Sellers PJ, Randall DA, Collatz GJ, Berry JA, Field CB, Dazlich DA, Zhang C, Collello GD, Bounoua L (1995b) A revised land surface parameterization (SiB2) for atmospheric GCMs. Part I: model formulation. J Clim 9:676–704

Sellers PJ, Dickinson RE, Randall DA, Betts AK, Hall FG, Berry JA, Collatz GJ, Denning AS, Mooney HA, Nobre CA, Sato N, Field CB, Henderson-Sellers A (1997) Modeling the exchanges of energy, water, and carbon between continents and the atmosphere. Science 275:502–509

Sharkey TD, Bernacchi CJ, Farquhar GD, Singsaas EL (2007) Fitting photosynthetic carbon dioxide response curves for C_3 leaves. Plant Cell Environ 30:1035–1040

Sieber A, Uhlenbrook S (2005) Sensitivity analyses of a distributed catchment model to verify the model structure. J Hydrol 310:216–235

Sobol' IM (1990) On sensitivity estimation for nonlinear mathematical models. Matematicheskoe Modelirovanie 2:112–118

Sobol' IM (1993) Sensitivity estimates for nonlinear mathematical models. Math Model Comput Exp 1:407–417

Sobol' IM (2001) Global sensitivity indices for nonlinear mathematical models and their Monte Carlo estimates. Math Comput Simul 55:271–280

Spiegelhalter DJ, Best NG, Carlin BP, van der Linde A (2002) Bayesian measures of model complexity and fit. J R Stat Soc Ser B 64:583–640

Su YH, Zhu GF, Miao ZW, Qi F, Chang ZQ (2009) Estimation of parameters of a biochemically based model of photosynthesis using a genetic algorithm. Plant Cell Environ 32:1710–1723

Su YH, Feng Q, Zhu GF, Gu CJ, Wang YQ, Shang SS, Zhang K, Han T, Chen HL, Ma JZ (2018) A hierarchical Bayesian approach for multi-site optimization of a satellite-based evapotranspiration model. Hydrol Process. https://doi.org/10.1002/hyp.13298

Tang Y, Reed P, van Werkhoven K, Wagener T (2007a) Advancing the identification and evaluation of distributed rainfall-runoff models using global sensitivity analysis. Water Resour Res 43:1–14

Tang Y, Reed P, Wagener T, van Werkhoven K (2007b) Comparing sensitivity analysis methods to advance lumped watershed model identification and evaluation. Hydrol Earth Syst Sci 11:793–817

Tcherkez GGB, Farquhar GD, Andrews TJ (2006) Despite slow catalysis and confused substrate specificity, all ribulose bisphosphate carboxylases may be nearly perfectly optimized. Proc Natl Acad Sci USA 103:7246–7251

Thornley JHM (1976) Mathematical models in plant physiology. Academic Press, London

Tomás M, Flexas J, Copolovici L, Galmés J, Hallik L, Medrano H, Ribas-Carbó Mique, Tosens T, Vislap V, Niinemets Ü (2013) Importance of leaf anatomy in determining mesophyll diffusion conductance to CO_2 across species: quantitative limitations and scaling up by models. J Exp Bot 64:2269–2281

Trudinger CM, Raupach MR, Peter JR, Kattge J, Liu Q, Pak B, Reichstein M, Renzullo L, Richardson AD, Roxburgh SH, Styles J, Wang YP, Briggs P, Barrett D, Nikolova S (2007) OptIC project: an intercomparison of optimization techniques for parameter estimation in terrestrial biogeochemical models. J Geophys Res 112:1–17

von Caemmerer S (2000) Biochemical models of leaf photosynthesis. Techniques in plant science, vol 2. CSIRO Publishing, Collingwood

von Caemmerer S, Farquhar GD (1981) Some relationships between the biochemistry of photosynthesis and the gas exchange of leaves. Planta 153:376–387

von Caemmerer S, Evans JR, Hudson GS, Andrews TJ (1994) The kinetics of ribulose-1,5-bisphosphate carboxylase/oxygenase in vivo inferred from measurements of photosynthesis in leaves of transgenic tobacco. Planta 195:88–97

Walker B, Ariza LS, Kaines S, Badger MR, Cousins AB (2013) Temperature response of *in vivo* Rubisco kinetics and mesophyll conductance in *Arabidopsis thaliana*: comparisons to *Nicotiana tabacum*. Plant Cell Environ 36:2108–2119

Walker AP, Ye M, Lu D, De Kauwe MG, Gu LH, Medlyn BE, Rogers A, Serbin SP (2018) The multi-assumption architecture and testbed (MAAT v1.0): R code for generating ensembles with dynamic model structure and analysis of epistemic uncertainty from multiple sources. Geosci Model Dev 11:3159–3185

Wang J, Li X, Liu L, Fang F (2013) Parameter sensitivity analysis of crop growth models based on the extended Fourier amplitude sensitivity test method. Environ Model Softw 48:171–182

Way DA, Yamori W (2014) Thermal acclimation of photosynthesis: on the importance of adjusting our definitions and accounting for thermal acclimation of respiration. Photosynth Res 119:89–100

Wright IJ, Reich PB, Cornelissen JHC, Falster DS, Garnier E, Hikosaka K, Lamont BB, Lee W, Oleksyn J, Osada N, Poorter H, Villar R, Warton DI, Westoby M (2005) Assessing the generality of global leaf trait relationships. New Phytol 166:485–496

Wullschleger SD (1993) Biochemical limitations to carbon assimilation in C_3 plants—a retrospective analysis of the A/C_i curves from 109 species. J Exp Bot 44:907–920

Wullschleger SD, Epstein HE, Box EO, Euskirchen ES, Goswami S, Iversen CM, Kattge J, Norby RJ, van Bodegom PM, Xu X (2014) Plant functional types in Earth system models: past experiences and future directions for application of dynamic vegetation models in high-latitude ecosystems. Ann Bot 114:1–16

Xu X, Liu X, Ge S, Jensen JD, Hu FY, Li X, Dong Y, Gutenkunst RN, Fang L, Huang L, Li JX, He WM, Zhang GJ, Zheng XM, Zhang FM, Li YR, Yu C, Kristiansen K, Zhang XQ, Wang Ji, Wright M, McCouch S, Nielsen R, Wang J, Wang W (2012) Resequencing 50 accessions of cultivated and wild rice yields markers for identifying agronomically important genes. Nat Biotechnol 30:105–111

Yamori W, Noguchi K, Terashima I (2005) Temperature acclimation of photosynthesis in spinach leaves: analyses of photosynthetic components and temperature dependencies of photosynthetic partial reactions. Plant Cell Environ 28:536–547

Zaehle S, Sitch S, Smith B, Hatterman F (2005) Effects of parameter uncertainties on the modeling of terrestrial biosphere dynamics. Glob Biogeochem Cycle 19:3020

Zhang C, Chu JG, Fu GT (2013) Sobol's sensitivity analysis for a distributed hydrological model of Yichun River Basin, China. J Hydrol 480:58–68

Zhang K, Ma JZ, Zhu GF, Ma T, Han T, Feng LL (2017) Parameter sensitivity analysis and optimization for a satellite-based evapotranspiration model across multiple sites using Moderate Resolution Imaging Spectroradiometer and flux data. J Geophys Res 122:230–245

Zhu GF, Li X, Su YH, Lu L, Huang CL (2011) Seasonal fluctuations and temperature dependence in photosynthetic parameters and stomatal conductance at the leaf scale of *Populus euphratica* Oliv. Tree Physiol 31:178–195